Astron. Astrophys. 362, 599–614 (2000)

ASTRONOMY AND ASTROPHYSICS

Neutron-capture nucleosynthesis in AGB stars

S. Goriely[1,⋆] **and N. Mowlavi**[2]

[1] Institut d'Astronomie et d'Astrophysique, C.P. 226, Université Libre de Bruxelles, 1050 Brussels, Belgium
[2] Observatoire de Genève, 1290 Sauverny, Switzerland

Received 31 January 2000 / Accepted 14 August 2000

Abstract. Recent AGB models including diffusive overshoot or rotational effects suggest the partial mixing (PM) of protons from the H-rich envelope into the C-rich layers during the third dredge-up. In order to study the impact of such a mixing on the surface abundances, nucleosynthesis calculations based on stellar AGB models are performed for different assumptions of protons (ranging from $X_{\rm p}^{\rm mix} = 10^{-6}$ to 0.7) in the PM zone. For high proton-to-^{12}C abundance ratios, light nuclei such as fluorine and sodium are efficiently produced, while heavier s-process nuclei are synthesized for lower proton-to-^{12}C ratios.

In the framework of the PM model, assuming a smooth exponentially decreasing proton profile, the surface ^{19}F abundance evolution is correlated with that of s-process nuclei in agreement with observations. However, as a function of the surface C/O abundance ratio, the surface ^{19}F enrichment remains difficult to reconcile with observations in AGB stars. Sodium is predicted to be efficiently produced in a small region of the PM zone with proton-to-^{12}C abundance ratio of about 10, but with large overproduction factors (up to fifty times higher than the sodium left over by the hydrogen burning shell).

The primary ^{13}C pocket formed in the PM zone at low proton-to-^{12}C ratios is responsible for an efficient production of s-process nuclei. A table of elemental overabundances predicted at the surface of AGB stars at four different metallicities is presented.

All the nucleosynthesis calculations are shown to suffer from major nuclear reaction rate uncertainties, in particular, $^{13}{\rm C}\,({\rm p}\,,\gamma)\,^{14}{\rm N}$, $^{14}{\rm N}\,({\rm n}\,,{\rm p})\,^{14}{\rm C}$ and $^{22}{\rm Ne}\,(\alpha\,,{\rm n})\,^{25}{\rm Mg}$. The major uncertainties associated with the amount of protons mixed into the C-rich zone are found in the extent of the PM zone rather than in the adopted H profile.

Finally, the PM scenario predicts that low-metallicity AGB stars enriched in s-process elements should exhibit a large overproduction of Pb and Bi compared to other s-isotopes. The search of such Pb-stars is highly encouraged.

Key words: nuclear reactions, nucleosynthesis, abundances – stars: abundances – stars: AGB and post-AGB

Send offprint requests to: S. Goriely
⋆ S.G. is FNRS Research Associate.

1. Introduction

The determination of chemical abundances at the surface of evolved stars provides important clues on both the structural evolution of those stars and on the interstellar abundance evolution. Among those stars, asymptotic giant branch (AGB) stars form an important class of objects for several reasons. They correspond to the late phase of the evolution of stars with masses between about 1 and $8\,{\rm M}_\odot$, which includes more than 80% of all stars; they exhibit peculiar surface abundances as compared to other red giant stars; and many of them are characterized by strong mass losses (up to $10^{-4}\,{\rm M}_\odot$ y^{-1}) which eject the surface material into the interstellar medium, contributing thereby to the galactic chemical evolution.

The abundance peculiarities observed at the surface of AGB stars are understood to result from the mixing at the surface of material synthesized in the deep layers (e.g Blöcker 1999, Lattanzio & Forestini 1999, Busso et al. 1999). This process is called the third dredge-up (denoted hereafter 3DUP). Nucleosynthesis can proceed through H-burning (affecting, among others, the CNO isotopes, ^{23}Na, or ^{26}Al) or, at still deeper layers, He-burning (producing, for example, ^{12}C and ^{22}Ne). Eventually, neutron-rich environments are found under some specific conditions in the He-burning layers and lead to the synthesis of ^{19}F and s-process elements. The $^{13}{\rm C}\,(\alpha\,,{\rm n})\,^{16}{\rm O}$ reaction is nowadays believed to be the major neutron source (Busso et al. 1999), while $^{22}{\rm Ne}\,(\alpha\,,{\rm n})\,^{25}{\rm Mg}$ becomes active in some, probably more massive, AGB stars. The efficiency of $^{13}{\rm C}\,(\alpha\,,{\rm n})\,^{16}{\rm O}$ depends on the uncertain availability of ^{13}C in sufficient amounts. A scenario has long been invoked to produce fresh ^{13}C by mixing protons from the envelope into the ^{12}C-rich layers during a 3DUP event (Iben & Renzini 1982), followed by the incomplete operation of the CN cycle of H-burning. The region over which the diffusive H mixing operates is called the 'partial mixing' (PM) zone in the present paper. Unfortunately, AGB models are still subject to large uncertainties concerning the consistent prediction of both the 3DUP and PM processes (e.g Mowlavi 1999a, Lattanzio 1998, Frost & Lattanzio 1996). In particular, the 3DUP and PM properties are expected to be sensitive to the stellar characteristics (such as the mass, metallicity or mass loss rate) or the numerical prescriptions used, in particular to describe the convective motions. The mixing scenario has recently been revived by the use of mechanisms, such as overshooting (Herwig et al. 1997) or rotation (Langer

et al. 1999). Models including such a diffusive mixing process, whether with overshooting or rotationally induced mixing, predict the formation of a ^{13}C pocket in a zone comprising some $10^{-5}\,M_\odot$ around the mass cut between the H-rich and C-rich layers. However, the total amount of ^{13}C produced in this way depends on the PM parameters (extent and efficiency of the overshoot, amplitude of rotation) which cannot be quantified ab initio at the present time. This leads to an uncertainty in the subsequent nucleosynthesis. One way to handle this problem at the moment is to assume some initial parametrized H abundance profile.

This paper studies in detail the nucleosynthesis operating in the PM zone and its consequences on the surface abundance predictions of AGB stars. Nucleosynthesis resulting from the partial mixing of protons into the C-rich region is followed during one representative interpulse and pulse phase of model stars of different masses ($M = 1.5$–$3\ M_\odot$) and metallicities ($Z = 0.001$–0.020). More specifically, we analyse the nucleosynthesis in the 15th thermal pulse cycle of a $1.5\,M_\odot$ $Z = 0.018$ star and the 20th of the $3\,M_\odot$ $Z = 0.020$, $2.5\,M_\odot$ $Z = 0.008$, $2.5\,M_\odot$ $Z = 0.004$ and $3\,M_\odot$ $Z = 0.001$ stars. All physical quantities in these representative pulse cycles (including the envelope mass) are taken from the evolutionary AGB models of Mowlavi (1995, 1999a,b). The mass region between the He-burning shell up to the bottom of the H-envelope is divided into about 400 zones. The nucleosynthesis in each zone is followed making use of the initial (at time of the 3DUP) abundances and temperature and density profiles given by evolutionary AGB models. Heavy elements are assumed to have an initial solar p and r pattern taken from Goriely (1999) with abundances scaled to the stellar metallicity $Z/Z_\odot$ (no prior abundance pollution with s-process nuclei is considered). In the pulse-driven convective region, the nucleosynthesis is calculated within the one-zone model, where the mean reaction *fluxes* are determined from the mass-averaged T-dependent rates over the whole convective region and the local abundances (only the neutron abundance is assumed not to be homogeneous, its abundances being estimated in each layer of the convective region from equilibrium between production and destruction rates). The nuclear reaction network includes about 530 nuclei up to Po with all relevant nuclear (n-, p-, α-captures), weak (electron captures, β-decays) and electromagnetic (photodisintegration) interactions. Nuclear reaction rates are taken from the Nuclear Astrophysics Library of the Brussels University (available at http://www-astro.ulb.ac.be), which includes the latest experimental cross sections and calculated rates within the statistical Hauser-Feshbach model (Goriely 1999). In particular, all the charged-particle-induced reaction rates of relevance in the H- and He-burning calculations presented here are taken from the recent European compilation of experimental rates, known as NACRE (Angulo et al. 1999). The β-decay and electron capture rates in stellar conditions are taken from Takahashi & Yokoi (1987). More details about the reaction network can be found in Goriely (1999). Note that the non-thermalization of the isomeric state in ^{85}Kr and ^{180}Ta, as well as the thermalization of ^{115}In and ^{176}Lu at temperatures exceeding $T_8 \simeq 2.5$[1] and $T_8 \simeq 3$, respectively, are introduced explicitly in the reaction network (Käppeler et al. 1989; Nemeth et al. 1994).

In Sect. 2, we perform an initial parametric study of nucleosynthesis of light and heavy (i.e heavier than iron) elements resulting from the partial mixing of protons into the C-rich zone for different amount of proton-to-^{12}C abundance ratios. The study covers proton-to-^{12}C ratios of about 0.1, known to be responsible for the s-process nucleosynthesis (Gallino et al. 1998), as well as ratios smaller and larger than that value, which have not been investigated yet in the framework of AGB models (Goriely & Molawi 2000). In Sect. 3, we assume a smooth exponentially decreasing H abundance profile in the PM zone, and follow the subsequent intershell nucleosynthesis for the representative interpulse-pulse phase in our different stars. In Sect. 4, surface abundance predictions are then analysed making assumptions regarding thermal pulse sequences, the mass extent of the PM and the mass processed by the 3DUP. The uncertainties in both the nuclear reaction rates and the adopted initial H-profile, and their impact on the nucleosynthesis predictions are analyzed in Sect. 5. The surface abundances predicted are compared with specific observations in Sect. 6. Some conclusions are finally drawn in Sect. 7.

2. Nucleosynthesis in the PM zone for different p to ^{12}C abundance ratios

Protons from the envelope are ingested artificially into the C-rich region (characterized by $X(^{12}\mathrm{C}) \simeq 0.23$) with a given mass fraction ranging from $X_\mathrm{p}^\mathrm{mix} = 10^{-6}$ up to 0.7 at the time of the 3DUP. The abundance of the other envelope elements is diluted proportionally to the proton abundance. The resulting nucleosynthesis is followed during the whole interpulse phase. Qualitatively, the nucleosynthesis is found rather insensitive to the depth to which protons are ingested. The composition of the C-rich region has indeed been homogenized by the preceeding pulse-driven convection and the interpulse nucleosynthesis is not very sensitive to the exact temperature and density conditions at which the protons are ingested. For this reason, the nucleosynthesis in the PM zone is analysed principally as a function of the abundance of the ingested protons $X_\mathrm{p}^\mathrm{mix}$.

2.1. H-burning

As already discussed by Jorissen and Arnould (1989), the nucleosynthesis occurring in the PM zone is extremely sensitive to the abundance X_p^mix of protons ingested therein At very low H abundances of $X_\mathrm{p}^\mathrm{mix} \lesssim 10^{-4}$ [corresponding to p to ^{12}C ratios $Y_\mathrm{p}/Y(^{12}\mathrm{C}) \lesssim 5\ 10^{-3}$, where $Y(A) = X(A)/A$ is the abundance of A by number], the number of protons captured by ^{12}C is too small to lead to any significant abundance modification.

At high H abundances of $X_\mathrm{p}^\mathrm{mix} \gtrsim 4 \times 10^{-2}$ [i.e. for $Y_\mathrm{p} \gtrsim 2 \times Y(^{12}\mathrm{C})$], there are enough protons to complete the CNO cycles leading to equilibrium abundances of the nuclei

[1] where T_8 is the temperature expressed in 10^8K

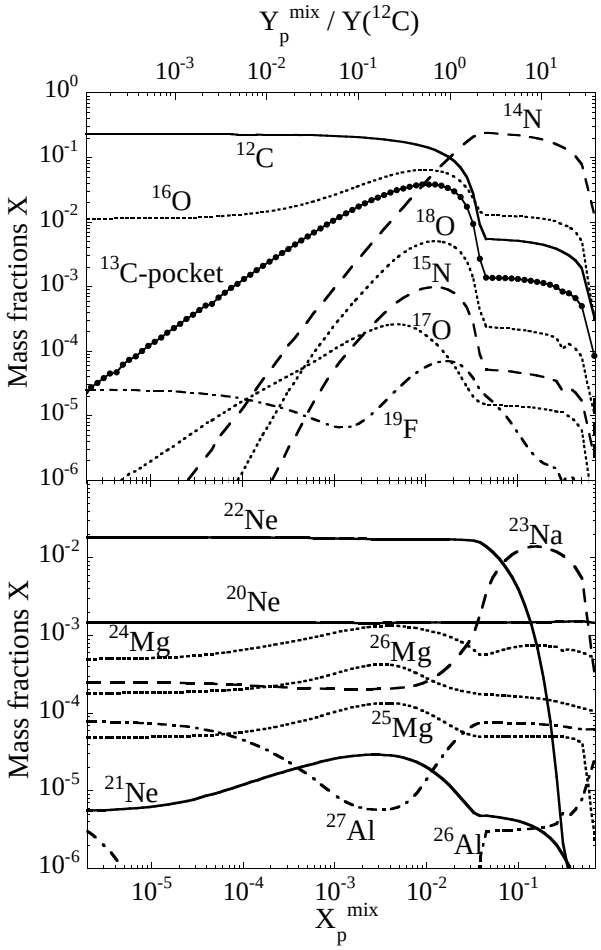

Fig. 1. Abundances of the elements from C to Al in the PM zone at the end of the 15th interpulse in a $1.5\,\mathrm{M}_\odot$ model star of solar metallicity. The abundances are expressed as a function of the initial H abundance in the PM zone. The C-rich layers of the model star are characterized by $X(^{12}\mathrm{C}) = 0.23$. The ^{13}C profile obtained at the end of the proton burning, but before the operation of $^{13}\mathrm{C}\,(\alpha\,,\mathrm{n})\,^{16}\mathrm{O}$, is also shown with the spherical dots. At the end of the interpulse, ^{13}C is totally destroyed.

involved in those cycles (cf. Fig. 1). This regime corresponds to the traditional H-burning nucleosynthesis operating in the H-burning shell (HBS), but with some peculiarities due to the high ^{12}C and ^{22}Ne enrichment in the PM zone. More specifically,

- ^{13}C is left over for $X_\mathrm{p}^\mathrm{mix} \simeq 10^{-2}$ at an abundance about fifty times higher than that from the HBS. This is the well-known (e.g Gallino et al. 1998) ^{13}C-pocket seen in Fig. 1;
- ^{23}Na is efficiently produced for $X_\mathrm{p}^\mathrm{mix} \simeq 10^{-1}$ by the NeNa cycle through $^{22}\mathrm{Ne}\,(\mathrm{p}\,,\gamma)\,^{23}\mathrm{Na}$ at an abundance up to fifty times higher than that in the HBS. The consequences of this high sodium production on the surface abundances are discussed in Sect. 4;
- ^{26}Al, which is synthesized in the MgAl cycle at temperatures above 35×10^6 K (e.g. Arnould et al. 1999), is found at the end of the interpulse phase to be lower by a factor of ten compared to its abundance from the HBS. This is due to its destruction, later during the interpulse, by the neutrons released by $^{13}\mathrm{C}\,(\alpha\,,\mathrm{n})\,^{16}\mathrm{O}$.

The intermediate regime of $10^{-4} \lesssim X_\mathrm{p}^\mathrm{mix} \lesssim 4\times10^{-2}$, [i.e. $0.005 \lesssim Y_\mathrm{p}/Y(^{12}\mathrm{C}) \lesssim 2$] is the richest from the nucleosynthesis point of view. In this regime ^{12}C is burned into ^{13}C by proton captures, but there are not enough protons to complete the CN cycle through $^{13}\mathrm{C}\,(\mathrm{p}\,,\gamma)\,^{14}\mathrm{N}$. A significant amount of ^{13}C is thus left over at the end of the proton captures and forms a ^{13}C pocket (Fig. 1). In comparison with the regime found for higher p to C ratios [at $Y_\mathrm{p}/Y(^{12}\mathrm{C}) \gtrsim 1$], the amount of primary[2] ^{13}C is not only larger, but the ^{14}N content is also sensitively smaller than the ^{13}C abundance.

The total amount of primary ^{13}C and ^{14}N produced in the intershell zone is of course expected to depend on the metallicity, since the extent of the PM zone and the initial H abundance mixed into the C-rich region are expected to vary with stellar mass, metallicity, and the physical mechanism responsible for the PM. However, it must be stressed that the amount of primary ^{13}C produced at a given layer depends only on the initial H and ^{12}C abundances in that layer[3]. As a result, the ^{13}C abundance profile, and thus the nucleosynthesis predictions in the PM zone, are, at this stage, independent of metallicity for identical proton mixing.

2.2. ^{13}C *burning*

When the temperature in the PM layers increases to about $T_8 \simeq 0.9$ later during the interpulse, the freshly produced ^{13}C burns and releases neutrons through $^{13}\mathrm{C}\,(\alpha\,,\mathrm{n})\,^{16}\mathrm{O}$. In contrast, ^{14}N is not affected by He-burning, because its α-capture rate is too low under the thermodynamic conditions encountered during the interpulse (typically, $T_8 \simeq 1$). The neutrons are mainly captured by $^{14}\mathrm{N}\,(\mathrm{n}\,,\mathrm{p})\,^{14}\mathrm{C}$, $^{16}\mathrm{O}(\mathrm{n},\gamma)^{17}\mathrm{O}(\mathrm{n},\alpha)^{14}\mathrm{C}$, $^{26}\mathrm{Al}\,(\mathrm{n}\,,\mathrm{p})\,^{26}\mathrm{Mg}$, and ^{56}Fe-peak nuclei through (n,γ) reactions. The latter captures initiate the production of heavy elements by the s-process, while captures by ^{14}N release ^{14}C and secondary protons of importance for light element nucleosynthesis.

For $X_\mathrm{p}^\mathrm{mix} \gtrsim 10^{-2}$, the neutrons are mainly captured by the abundant ^{14}N leading to the production of ^{18}O by $^{14}\mathrm{N}(\mathrm{n},\mathrm{p})^{14}\mathrm{C}(\alpha,\gamma)^{18}\mathrm{O}$. The subsequent release of protons also favours the synthesis of ^{15}N through $^{18}\mathrm{O}\,(\mathrm{p}\,,\alpha)\,^{15}\mathrm{N}$ (Fig. 1). Note that the production of ^{18}O results from the α-capture on ^{14}C and not ^{14}N, and consequently follows the ^{13}C (i.e the neutron), and not the ^{14}N, profile (Fig. 1)[4]. The production of ^{15}N

[2] An element is said to be *primary* if it can be synthesized in a zero metallicity star. In contrast, an element is said to be *secondary* if its synthesis is related to the presence of some elements heavier than helium in the initial stellar composition.

[3] Note that diffusive overshoot can also give rise to an extension of the pulse-driven convective zone towards deep layers below the He-shell, and consequently, to an increase of the intershell abundance of ^{12}C (Herwig et al. 1999a)

[4] The $^{14}\mathrm{C}\,(\alpha\,,\gamma)\,^{18}\mathrm{O}$ rate at the typical interpulse temperature of $T_8 = 1$ in the PM zone is about 6 orders of magnitude larger than the $^{14}\mathrm{N}\,(\alpha\,,\gamma)\,^{18}\mathrm{F}$ rate.

is of particular interest, since it is at the origin of the possible ^{19}F nucleosynthesis by $^{15}\mathrm{N}\,(\alpha\,,\gamma)\,^{19}\mathrm{F}$ in the subsequent pulse driven convective zone (see Sect. 3).

For lower proton to ^{12}C ratios ($X_{\rm p}^{\rm mix} \simeq 10^{-3}$), neither ^{14}N nor ^{26}Al are abundant enough to be efficient neutron poisons. In these conditions, neutrons are mainly captured by the iron group nuclei leading to an efficient s-process nucleosynthesis. The fraction of neutrons effectively captured by nuclei heavier than iron and responsible for the s-processing is measured by (Iben & Renzini, 1982) $R = \sum_{A\geq 56}\langle\sigma\rangle_A Y(A)/\sum_A\langle\sigma\rangle_A Y(A)$, where $\langle\sigma\rangle_A$ is the Maxwellian-averaged neutron capture cross section of element of mass A. The s-process *strength* is characterized by $\int_0^t R(t)\ N_{\rm n}(t)\ v_T(t)\ dt$ which can be approximated by $R\times\tau$, where $\tau = \int_0^t N_{\rm n}\ v_T\ dt$ is the well-known time-integrated neutron exposure ($N_{\rm n}$ is the neutron density and v_T the most probable relative neutron-nucleus velocity at temperature T). Another quantity of relevance to characterize the s-process strength is the number $n_{\rm cap}$ of neutrons captured by the heavy elements (i.e. iron group nuclei) per heavy nucleus. Formally, $n_{\rm cap}$ is defined by $\sum_{A\geq 56} A\ \bar{Y}(A) - \sum_{A\geq 56} A\ \bar{Y}_0(A)$, where $\bar{Y}(A)$ is the abundance of isotope A normalized to $\sum_{A\geq 56}\bar{Y}(A) = 1$, and $\bar{Y}_0(A)$ its initial abundance. The quantity $n_{\rm cap}$ almost univoquely determines the s-process abundance distribution (with the exception of branching nuclei the abundance of which also depends on the temperature of the s-process). The higher $n_{\rm cap}$, the stronger the s-process. As shown in Fig. 2 (see also Fig. 7–22 of Clayton 1983), a value of $n_{\rm cap} \simeq 40$ leads to the synthesis of elements between Zr and Ba, while $n_{\rm cap} \simeq 140$ implies a large overproduction of Pb and Bi nuclei. Intermediate values of $n_{\rm cap} \simeq 60$ lead to the production of almost all nuclei within the main s-component ($90 \lesssim A \lesssim 204$).

The quantities τ and $n_{\rm cap}$ at the end of the interpulse period, as well as R during the neutron irradiation are displayed in Fig. 3 as a function of the initial H abundance for stars of different metallicities. Fig. 3 illustrates the remarkable sensitivity of the s-process to the stellar metallicity and to the number of protons mixed in the C-rich layers. Contrary to the production of primary ^{13}C and light neutron poisons (for given initial H abundance profiles, of course), the s-process is very sensitive to the stellar metallicity Z for the simple reason that the seed (mainly iron) abundance is proportional to Z, while the primary ^{13}C abundance is metallicity-independent (see also Gallino et al. 1998). As a result, the neutron to seed abundance ratio is inversely proportional to Z, and $n_{\rm cap}$ increases with decreasing metallicities up to a maximum value of $n_{\rm cap} \simeq 150$ corresponding to the transmutation of all seed nuclei into Pb and Bi, the heaviest elements possibly produced by the s-process. For the same reason, the neutron density reaches maximum values of about $N_{\rm n} = 10^7\ \mathrm{cm}^{-3}$ at solar metallicities, while it reaches $10^9\ \mathrm{cm}^{-3}$ at $Z = 0.001$. The neutron exposure is consequently much higher in a low-metallicity star. However, the efficiency of the neutron capture by the heavy seed nuclei R decreases with decreasing metallicity (reaching at most 70% in solar metallicity stars and 30% in $Z = 0.001$ stars). This shows that the impact of the light poisons (mainly ^{14}N) increases with decreasing metallicities. The pollution of the PM zone by an envelope enriched in N (produced by hot bottom burning, for example) could increase the poisons abundance in the PM zone, and therefore decrease even more $n_{\rm cap}$. In this case, stars of similar metallicity would experience different s-process strengths depending on the envelope's composition, even for a similar partial ingestion of protons.

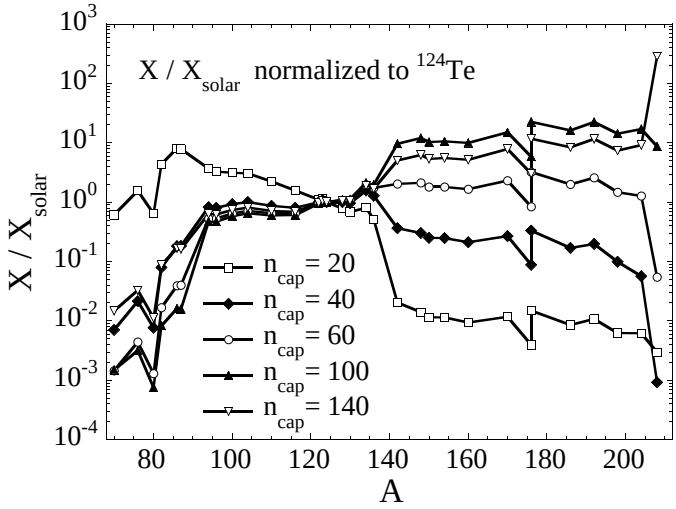

Fig. 2. Abundance distribution (relative to solar) of s-only nuclei corresponding to given values of the number $n_{\rm cap}$ of neutrons captured by the iron-group nuclei. All distributions are normalized to $X/X_\odot = 1$ for ^{124}Te. Each curve is obtained from an initial proton-to-^{12}C abundance ratio in the PM zone leading to the refered s-process strength $n_{\rm cap}$ (see also Fig. 3c). The curves include ^{208}Pb, but not some temperature-dependent branching nuclei, such as ^{152}Gd, ^{164}Er or ^{187}Os, which are sensitive to the exact thermodynamic conditions in the PM zone.

Let us finally note that the s-process strength is almost independent of the thermodynamic profiles in the intershell layers. Indeed, the number of neutrons captured by the heavy nuclei is fixed by the amount of primary ^{13}C available, and remains insensitive to the exact temperature at which ^{13}C burns. Therefore, Fig. 3 is independent of the stellar mass considered.

3. Intershell nucleosynthesis resulting from an H abundance profile in the PM zone

So far, we studied the interpulse nucleosynthesis resulting from the partial mixing of a given amount of protons into the C-rich region. The overshooting or rotational AGB models qualitatively predict the partial mixing of protons to be less effective when going deeper into the star (no definite quantitative results are available at the moment). To simulate these predictions, we arbitrarily adopt an initial (i.e at the moment of the 3DUP) H abundance profile in the PM region which exponentially decreases with depth from $X_{\rm p}^{\rm mix} = 0.7$ at the bottom of the convective envelope to 10^{-6} at the bottom of the PM zone. The abundance of the other envelope elements is diluted proportionally to the proton abundance in each layer. It seems reasonable to believe that the H abundance profile in the PM zone follows

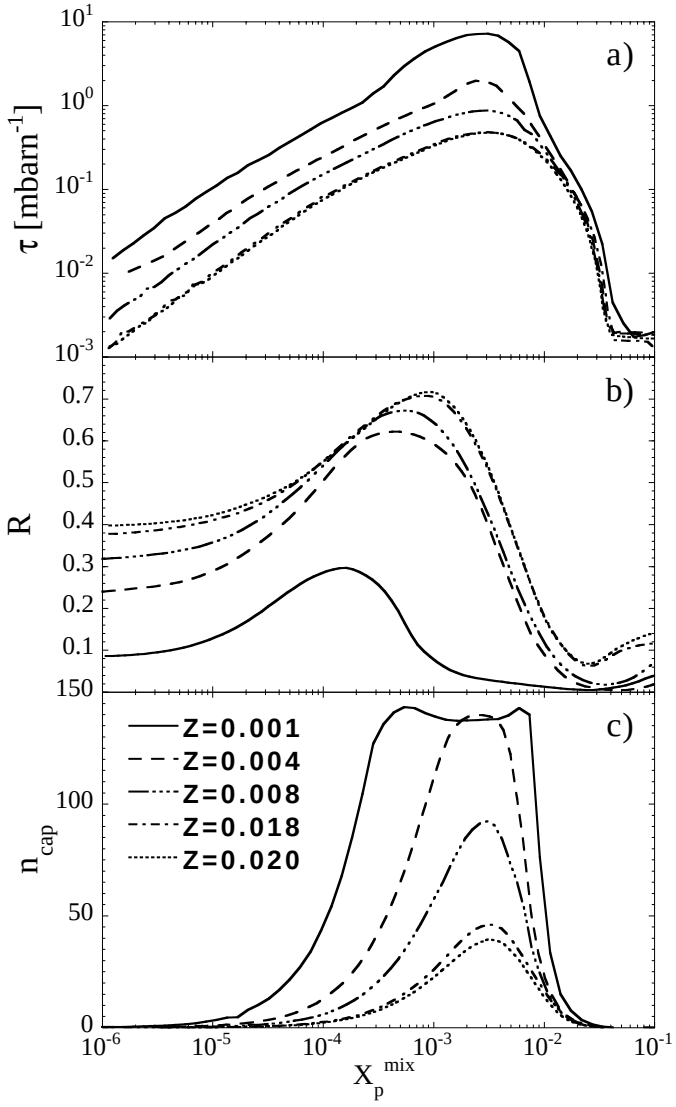

Fig. 3a–c. Neutron exposure τ at the end of the interpulse period **a**, the number of neutrons captured by the heavy nuclei relative to the total released R during the s-process **b** and the number of neutrons captured per seed nucleus $n_{\rm cap}$ at the end of the interpulse period **c** in stars of different metallicities Z as a function of the proton mass fraction $X_{\rm p}^{\rm mix}$ initially mixed into the C-rich layers.

a smooth and monotonic decreasing pattern with depth, if it results from some diffusion process [Herwig et al. 1999b; see also Asida and Arnett (2000) for overshoot simulations in two-dimensional models]. But there is of course no physical reason to believe that it would follow an exponential shape. Yet, as shown in Sect. 2, the most relevant nucleosynthesis in the PM zone occurs in layers where $X_{\rm p}^{\rm mix}$ lies between 10^{-3} and 10^{-1} ($X_{\rm p}^{\rm mix} \simeq 10^{-3}, 10^{-2}, 10^{-1}$ are found to be responsible for the the production of s-elements, ^{19}F and ^{23}Na, respectively). In that restricted range, it is more likely that the actual profile can be approximated by an exponential function (see for example the profile predicted by the overshoot model of Herwig et al. 1999b). The impact of our assumptions regarding the H profile on the s-process nucleosynthesis is investigated in Sect. 5.2.

We characterize the extent of the PM zone (of mass $M_{\rm pm}$) by $\lambda_{\rm pm} = M_{\rm pm}/M_{\rm Pulse}$ (where $M_{\rm Pulse}$ is the mass processed by the pulse-driven convection zone). We assume a standard value of $\lambda_{\rm pm} = 0.05$. Note that the adopted 5% extension of the PM zone with respect to the pulse region could seem relatively large compared with the predicted values (roughly $M_{\rm pm} \simeq 10^{-5}\,{\rm M}_\odot$; Herwig et al., 1999b) obtained within the overshooting or rotational models, but such a high value is required if any enrichment of the stellar surface is to be observed (see Sect. 6). It should also be kept in mind that the PM extension is defined here as the region where $X_{\rm p}^{\rm mix}$ decreases from 0.7 to 10^{-6}. As shown in Sects. 2 and 5.2, the so-called ^{13}C pocket which actually leads to the s-process development is predicted to cover a region about 5 to 20 times smaller than the PM zone.

The scenario adopted here is in many ways similar to the work of Gallino et al. (1998). There are, however, major differences between both approaches. First, Gallino et al. start with a H abundance profile to estimate the initial ^{13}C and ^{14}N pocket required *"to reproduce the main component and to match spectroscopic observation of s-enhanced stars"* and concentrate on the s-process nucleosynthesis only. We start the nucleosynthesis from a H abundance profile, logically (though arbitrarily) assuming that it decreases smoothly with depth without further pre-defined assumptions on its profile. We then consistently follow the resulting synthesis of all, light and heavy, nuclei. Second, we investigate the whole range $10^{-6} \leq X_{\rm p}^{\rm mix} \leq 0.7$, while Gallino et al. restrict themselves to the range $2\,10^{-4} \leq X_{\rm p}^{\rm mix} \leq 2\,10^{-3}$. As shown in Sect. 2, the $10^{-2} \lesssim X_{\rm p}^{\rm mix} \lesssim 10^{-1}$ regime is important for the nucleosynthesis of some light elements (^{15}N, ^{23}Na, cf Fig. 1) and the partial mixing of protons with $X_{\rm p}^{\rm mix} \lesssim 2\,10^{-4}$ (in the case of low-Z stars) or $X_{\rm p}^{\rm mix} \gtrsim 2\,10^{-3}$ also contributes to the production of s-elements (Fig. 3).

Assuming an exponentially decreasing H profile at the moment of the 3DUP, the PM zones of stars of different metallicities are found to be enriched, at the end of the interpulse phase, with the s-abundance distributions shown in Fig. 4. All stars, irrespective of their metallicity, are expected to produce the interpulse elements with $90 \lesssim A \lesssim 140$ with an almost solar distribution pattern. In contrast, only low-metallicity stars ($Z \lesssim 0.01$) are predicted to synthesize heavier s-nuclei ($140 \lesssim A \lesssim 204$) efficiently. Of particular interest is also the large overproduction of Pb and Bi for stars with metallicities $Z \lesssim Z_\odot/10 = 0.002$. These results are consistent with the abundance distributions obtained by Gallino et al. (1998) and Travaglio et al. (1999). The low-T ($T_8 \simeq 1$) s-process taking place during the radiative interpulse phase also leads to a strong under- or over-production of some temperature-dependent branching s-nuclei. In particular, this is the case of ^{164}Er or ^{187}Os which are underproduced by factors of about 10 to 100 compared with neighbouring s-only nuclei and of ^{152}Gd which is about 10 times more overproduced than ^{154}Gd.

The ashes of the radiative nucleosynthesis during the interpulse phase are ingested into the pulse-driven convective region and mixed down to the high temperatures T_p characterizing its base. T_p is well known to increase with increasing pulse num-

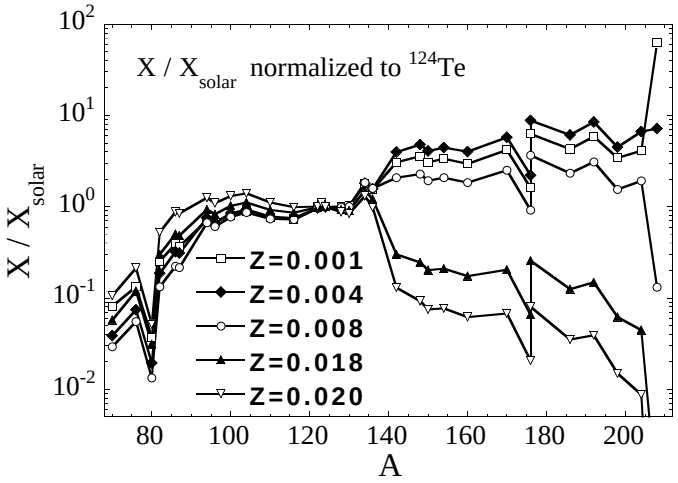

Fig. 4. Abundance distribution (relative to solar) of s-only nuclei at the end of one interpulse phase for stars of different metallicities. The distribution is averaged over the mass range covered by the PM region (assuming an initial exponentially decreasing H profile) and normalized to the solar abundance of ^{124}Te. Some T-dependent branching nuclei, such as ^{152}Gd, ^{164}Er or ^{187}Os, are not represented for the sake of clarity.

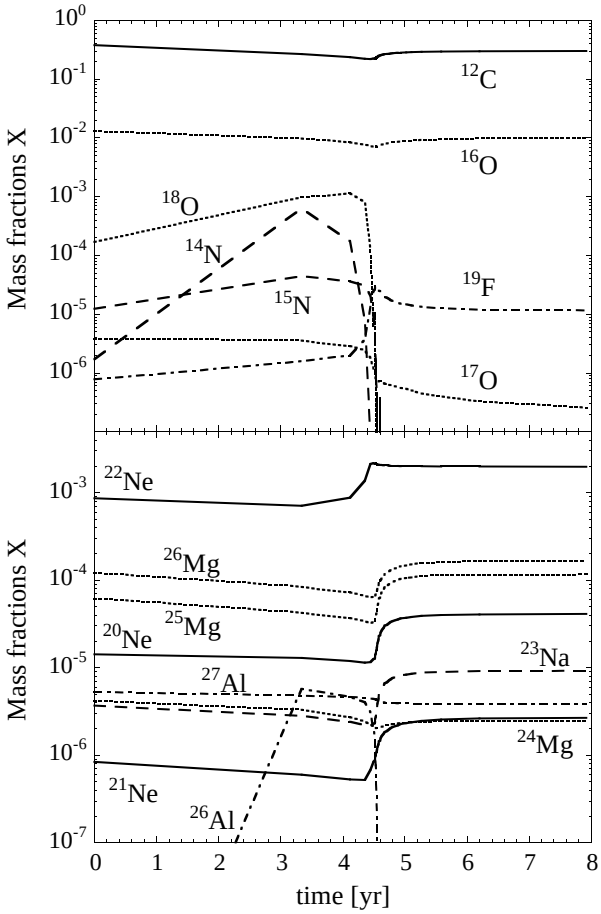

Fig. 5. Time evolution of the light elements mass fractions during the convective nucleosynthesis in the 20th pulse of a $3\,M_\odot$ $Z = 0.001$ star (T_p reaches 3.2×10^8 K). The increase of the mass fractions at early times corresponds to the element ingestion into the pulse during its outward extension.

ber, stellar mass or decreasing metallicity, and ranges from 1.5 to above 3×10^8 K (e.g. Boothroyd & Sackmann 1988). At these high temperatures, the ^{14}N and ^{18}O left over by the HBS during the preceding interpulse are completely transformed into ^{22}Ne by α-capture reactions. At temperatures $T_p \gtrsim 2.7\times10^8$ K (found in low-Z and/or high-M stars), $^{22}\mathrm{Ne}(\alpha,\mathrm{n})^{25}\mathrm{Mg}$ becomes fast enough to burn ^{22}Ne partially, and to be at the origin of a second neutron burst (Gallino et al. 1998). This second neutron burst takes place during a relatively short period of time (several years), but reaches much higher densities as compared to the first neutron irradiation during the interpulse.

The abundance distribution of the light nuclei resulting from the α- and n-capture reactions in the hot pulse of a low-metallicity ($Z = 0.001$) star is shown in Fig. 5. Besides the ^{22}Ne increase mentioned above and its partial destruction by α-captures (by about 4% in the case shown in Fig. 5), ^{19}F is seen to be efficiently produced by $^{15}\mathrm{N}\,(\alpha\,,\gamma)\,^{19}\mathrm{F}$. The production of ^{19}F is metallicity independent, since the neutrons and protons required for the synthesis of ^{15}N are produced in the PM zone by primary ^{13}C and ^{14}N, respectively. This primary ^{19}F adds to the secondary ^{19}F produced from the ashes of the He-burning shell (which is non-negligible only in solar or above-solar metallicity stars, cf. Mowlavi et al. 1996). The various neutron captures on nuclei such as ^{19}F, ^{20}Ne, ^{22}Ne following the ^{22}Ne-burning also contribute significantly to the increase of the ^{20,21}Ne, ^{23}Na abundances by a factor of about two to four (Fig. 5).

The global s-abundance distribution is only slightly affected by this second neutron irradiation, because only a few neutrons are captured per heavy seed nucleus (at least when use is made of the recommended NACRE reaction rates; see Sect. 5). However, locally, two major effects on the heavy nuclei abundances are found (Fig. 6). The first concerns the modification of the abundances of the so-called T-dependent s-branching nuclei, e.g ^{164}Er, ^{187}Os and ^{205}Pb, due to high temperatures found in the pulse driven convective zone. Second, the high neutron densities encountered at the time of maximum pulse extension ($N_\mathrm{n} \simeq 10^{12}\mathrm{cm}^{-3}$) leads to the destruction of some s-only nuclei (e.g ^{142}Nd) and the synthesis of some sr-nuclei by short-cutting the s-process flow if the neutron capture becomes faster than the β-decay. In particular, sr-nuclei in the $A \simeq 90, 120, 140, 180, 205$ regions are found to be produced in an almost solar ratio similarly to the s-only nuclei. Some elements like ^{96}Zr or ^{142}Ce are even overproduced. In contrast, in all the model stars considered here, ^{115}Sn and ^{180}Ta are significantly underproduced by factors of about 10 and 1000, respectively, with respect to their s-only neighbours. If the PM scenario of the s-process is confirmed, ^{115}Sn and ^{180}Ta should not be considered as s-nuclei[5], in disagreement with the canonical model conclusions (e.g. Goriely 1999).

[5] Note that the production of ^{115}Sn can be partially explained by the r-process (Nemeth et al. 1994) and ^{180}Ta by the p-process (Rayet et al. 1995).

The nucleosynthesis results presented here depend on the temperature (and in particular T_p) and density profiles in the He-flash convective zone. In addition to the well-known stellar mass and metallicity dependence of these profiles (e.g Boothroyd & Sackmann 1988), diffusive overshoot can also modify the structure of the pulse-driven convective zone by extending its base towards deeper layers, and thereby increasing T_p (Herwig et al. 1999a). This would not only favour the operation of the $^{22}\mathrm{Ne}(\alpha,\mathrm{n})^{25}\mathrm{Mg}$ neutron source during the pulse phase, but also mix elements synthesized in the deep layers into the intershell convective zone. This mixing could even include s-process nuclei resulting from the radiative $^{22}\mathrm{Ne}(\alpha,\mathrm{n})^{25}\mathrm{Mg}$ burning during the interpulse phase.

4. Surface abundance predictions

The quantitative prediction of AGB surface abundances is affected by the uncertainties of their structural evolution. Those uncertainties mainly concern the PM characteristics and the 3DUP efficiency. In addition to the basic assumptions made regarding the H abundance profile and extent of the PM zone (Sect. 3), we now assume a constant 3DUP efficiency. The 3DUP efficiency is traditionally measured by the parameter $\lambda = M_{\mathrm{dup}}/M_{\mathrm{H}}$, where M_{dup} is the amount of matter dredged-up after a pulse, and M_{H} is the amount of matter processed by the HBS between two successive pulses. In this study, we rather quantify the 3DUP efficiency by the parameter $\lambda_{\mathrm{dup}} = M_{\mathrm{dup}}/M_{\mathrm{Pulse}}$. It represents the mass fraction of the pulse driven convective zone which is dredged up. It can be written in terms of the classical parameter λ as $\lambda_{\mathrm{dup}} = \lambda \times M_{\mathrm{H}}/M_{\mathrm{Pulse}}$, where the ratio $M_{\mathrm{H}}/M_{\mathrm{Pulse}}$ varies smoothly between about 0.1 and 0.6 (cf. Fig. 8b of Mowlavi 1999b). In the present study, we assume a constant value of $\lambda_{\mathrm{dup}} = 0.1$ from one pulse to the next. Since the amount of C-rich material mixed to the surface is directly proportional to λ_{dup}, the surface chemical enrichment as a function of time is dependent on that parameter too. We can, to some extent, bypass this difficulty by expressing the surface abundances as a function of the surface $^{12}\mathrm{C}$ mass fraction, the latter being a direct product of the He-burning shell. The predictions obtained by the assumption of constant dredge-up efficiency are only approximate, because the intershell characteristics (temperature, density, PM and 3DUP parameters) do vary with time along the AGB, and consequently affect part of the intershell nucleosynthesis.

Finally, we assume that the AGB star experiences a sequence of identical interpulse-pulse phases (corresponding to the representative sequence studied so far) with constant envelope mass and PM and 3DUP characteristics pulse after pulse, all characterized by the same thermodynamic conditions and nucleosynthesis history. We neglect the feedback of the 3DUP on the intershell nucleosynthesis and the repeated neutron exposition due to the overlap of thermal pulses. Regarding the s-process, the latter two assumptions are justified if small λ_{pm}-values are considered. Indeed, if we consider the illustrative case of the $1.5\,\mathrm{M}_\odot$ model star of solar metallicity, the mass fraction of the s-process elements left over in the intershell region after one thermal pulse cycle (with $\lambda_{\mathrm{pm}} = 0.05$) reach about $2.5\ 10^{-5}$. This value is to be compared with the solar mass fraction of the Fe-group nuclei of about $1.4\ 10^{-3}$ and corresponds to an abundance (by number) ratio of Fe to heavy elements of roughly 100. Therefore, the iron-group nuclei remain the dominant neutron absorbers among the heavy nuclei inhibiting significant repeated neutron captures by s-nuclei from one pulse to the next. However, our simplifying assumptions are not adequate to follow the light elements which are predominantly produced in the HBS and which are sensitive to the intershell thermodynamic conditions and/or 3DUP feedbacks (for example $^{26}\mathrm{Al}$, cf. Mowlavi & Meynet 2000).

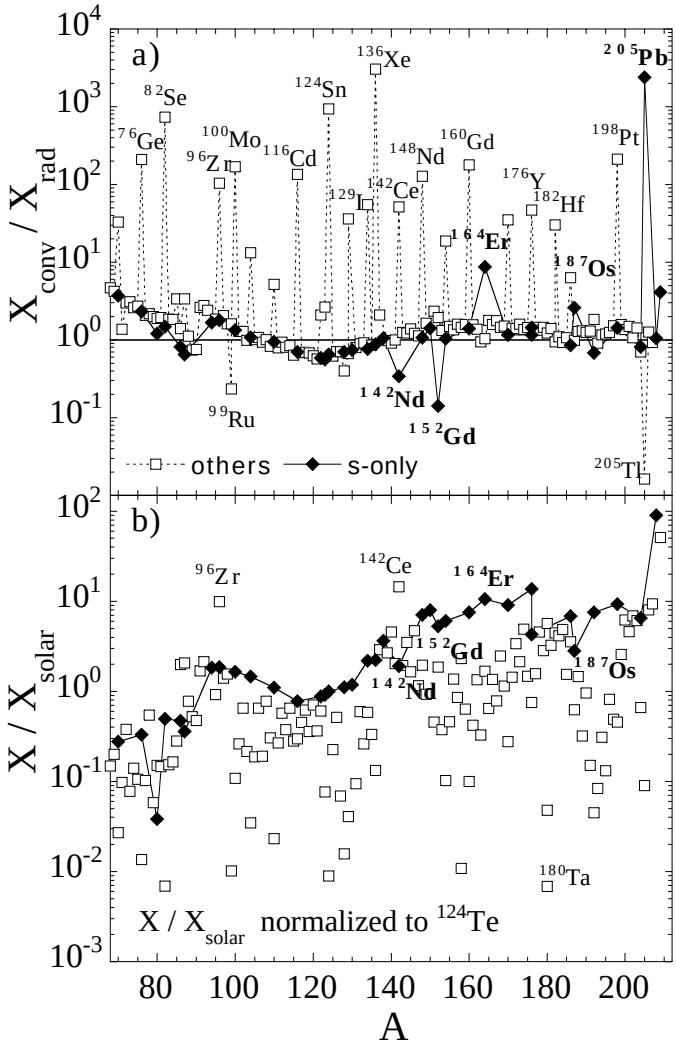

Fig. 6. a Impact of $^{22}\mathrm{Ne}(\alpha,\mathrm{n})^{25}\mathrm{Mg}$ on the heavy elements abundances in the 20th pulse of a $3\,\mathrm{M}_\odot$ $Z = 0.001$ star (T_p reaches 3.2×10^8 K). $X_{rad}(X_{conv})$ is the mass fraction at the end of the radiative interpulse (convective pulse). S-only isotopes are connected by a full line and printed in bold. **b** Abundance distribution (relative to solar) at the end of the convective pulse phase for the same star as in **a**. The distribution is normalized to the solar abundance of ^{124}Te.

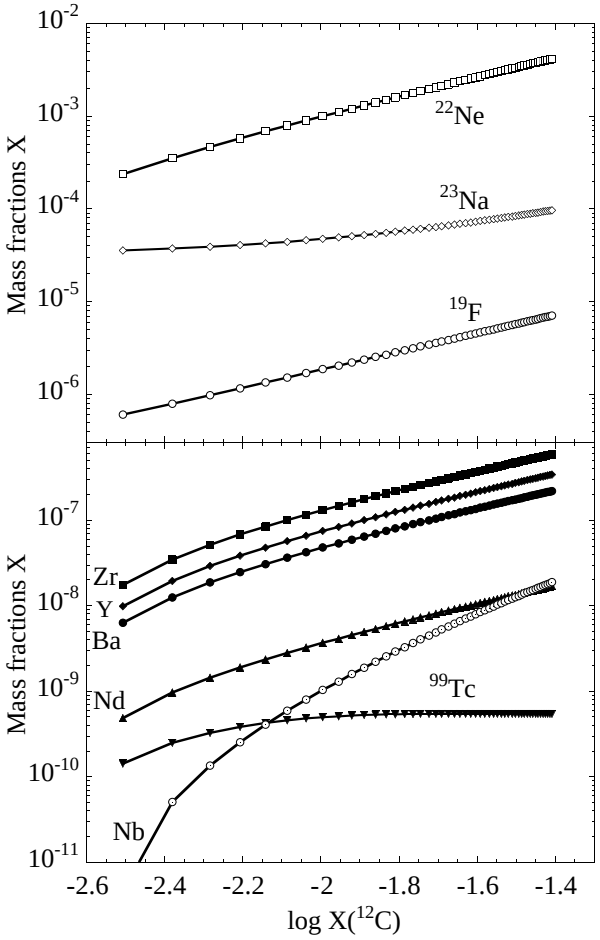

Fig. 7. Abundance evolution of several light (upper pannel) and heavy (lower pannel) elements as a function of the carbon abundance predicted at the surface of a $1.5\,\mathrm{M}_\odot$ star of solar metallicity. The 3DUP and PM parameters are $\lambda_{\rm dup} = 0.10$ and $\lambda_{\rm pm} = 0.05$, respectively. Each symbol corresponds to one thermal pulse cycle.

4.1. Light elements

Among the elements which are significantly affected by the PM nucleosynthesis, ^{19}F and ^{23}Na are of particular interest (Fig. 7). ^{23}Na is known to be efficiently produced in the HBS after a sufficient amount of carbon has been dredged-up to the surface (Mowlavi 1999b). This is due to the 3DUP feedbacks which progressively enrich the envelope with ^{22}Ne. Our analysis shows that the PM zone can be an additional source of sodium production (Sect. 2) thanks to the diffusive mixing of protons into the ^{22}Ne-rich layers. Although the production of ^{23}Na occurs only in a small fraction of the PM zone, the large mass fractions of $X(^{23}\mathrm{Na}) \simeq 10^{-2}$ (i.e about 50 to 100 times more than in the HBS without 3DUP feedback) reached around $X_{\rm p}^{\rm mix} \simeq 0.2$ (Fig. 1) can significantly contribute to the surface enrichment. The resulting surface abundance evolution is shown in Fig. 7 as a function of surface ^{12}C abundance. This sodium abundance adds to that predicted by the 3DUP feedbacks (Fig. 6 of Mowlavi 1999b).

Similarly, the PM of protons into the C-rich layers can significantly enrich the surface of AGB stars in ^{19}F. Without the PM mechanism, only a small amount of ^{19}F can be produced from secondary ^{13}C in the intershell layers (Mowlavi et al. 1996). A high production of ^{19}F is actually suggested by the observation of large fluorine overabundances at the surface of AGB stars (Jorissen et al. 1992). The fact that those overabundances are found to be correlated with s-process overabundances further supports the PM scenario and can put some constraint on the $X_{\rm p}^{\rm mix}$ range: the simultaneous production of ^{15}N (the progenitor of ^{19}F) and s-process nuclei requires H mixing with $10^{-3} \lesssim X_{\rm p}^{\rm mix} \lesssim 3 \times 10^{-2}$ (cf. Figs. 1,3).

4.2. S-process nuclei

The surface abundance evolution of some s-only elements, frequently observed at the surface of AGB stars, is shown in Fig. 7. Most of the s-elements present the same evolution pattern corresponding to their dilution from the pulse driven convective zone into the envelope by the successive 3DUPs. However, of particular interest (Smith and Wallerstein 1983, Takahashi et al. 1986, Busso et al. 1992) is the time evolution of the surface abundance of ^{99}Tc, the longest lived Tc isotope produced by the s-process, which has a half-life (2.1×10^5 yr) of the order of the interpulse period. In stars with short interpulse phases (10^4 yr), the increase in the ^{99}Tc abundance due to the 3DUP is higher than the decrease through β-decay, and the surface abundance slightly increases with time. Stars with longer interpulse phases (10^5 yr), however, experience more ^{99}Tc decay between two successive 3DUPs, and keep a constant mean ^{99}Tc abundance at their surface. This time-independent property of ^{99}Tc can be of great interest in the comparison of model predictions with observations, as discussed in Sect. 6. Note that none of our calculations predicts the ^{99}Tc β-decay during the convective pulse. Although high temperatures strongly shorten the ^{99}Tc half-live ($\tau_{1/2} = 4.5$ yr at $T_8 = 3$), this reduction does not endanger its survival.

A complementary pattern, compared with the Tc one, is found for the surface enrichment in Nb (Fig. 7). Nb is exclusively produced by the decay of ^{93}Zr ($\tau_{1/2} = 1.5\ 10^6$ yr). Therefore, Nb fully populates the stellar surface only million years after s-process elements have been dredged-up. The surface abundance of Nb is expected to be anti-correlated with the Tc abundance.

The stellar metallicity plays a fundamental role in the yields of heavy elements. Fig. 8 presents the surface abundance distribution of s-only isotopes predicted after a series of 30 identical thermal pulse cycles in five AGB models of different masses and metallicities, and with the assumptions described above. Qualitatively, the surface s-abundance distributions are similar to those predicted in the PM region at the end of the interpulse phase (Fig. 4), namely the synthesis of $90 \lesssim A \lesssim 140$ nuclei in solar metallicity stars, of $90 \lesssim A \lesssim 204$ nuclei in $Z \leq Z_\odot/2 = 0.01$ and a strong overproduction of Pb and Bi in low-Z AGB stars ($Z \lesssim 0.001$). If the standard s-process scenario described here is valid, high amounts of Pb should be ob-

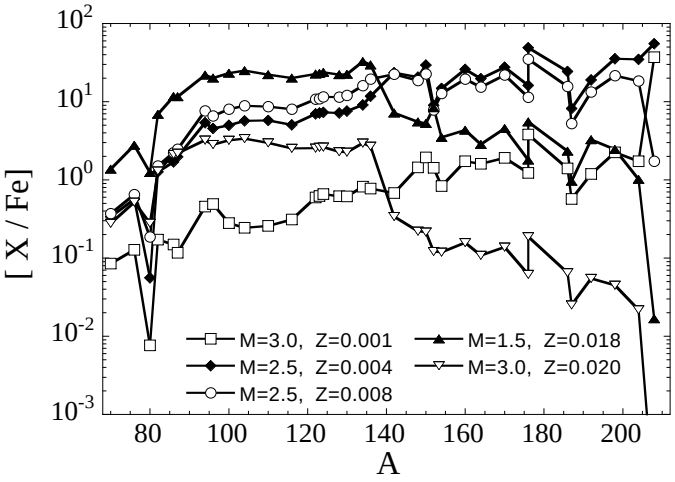

Fig. 8. Surface overproduction factors (with respect to solar) of s-only isotopes after the onset of 30 dredge-ups in five AGB model stars, as labelled in the figure.

served in low-Z AGB stars (which could be called "Pb-stars"). Inversely, if low-Z AGB stars enriched in s-process nuclei do not show any Pb overabundance, then the standard PM scenario must be reexamined in depth.

Table 1 gives the elemental overabundances [el/Fe] characteristic of the matter dredged-up and found at the surface after a series of 10, 30 and 50 identical interpulse/pulse/dredge-up sequences in four AGB stars of different metallicities and for DUP and PM parameters $\lambda_{\rm dup} = 0.10$ and $\lambda_{\rm pm} = 0.05$[6]. The predictions for different pulse numbers given in Table 1 represent different degrees of dilution due to different values of the number of thermal pulse cycles, the envelope mass ($M_{\rm env}$), $\lambda_{\rm pm}$ or $\lambda_{\rm dup}$. The degree of stellar surface enrichment predicted for heavy elements differs for s-only, s-dominant or r-dominant elements, since all elements have different s-contribution to the solar system abundance[7]. These data could help astronomers to estimate unobserved abundance ratios in a way similar to Malaney's table (1987). These predictions are subject to the uncertainties discussed in Sect. 5.

The surface overproduction factors (relative to solar) obtained for s-nuclei (and ^{19}F) depend on two major dilution effects: that of the PM zone into the pulse (described by $\lambda_{\rm pm}$), and that of the dredged-up matter into the envelope (given by $M_{\rm dup}/M_{\rm env} = \lambda_{\rm dup} \times M_{Pulse}/M_{\rm env}$). Low-$M$, high-$Z$ AGB stars have, relatively, small envelope masses and intershell convective zones with large masses, i.e large $M_{\rm Pulse}/M_{\rm env}$ ratios (a $6M_\odot$ star has for example an average $M_{\rm Pulse}/M_{\rm env}$ ratio which is about 100 times smaller than in a $1.5M_\odot$ star). Therefore, for fixed $\lambda_{\rm pm}$ and $\lambda_{\rm dup}$ parameters, one may expect the surface overproduction factors to be smaller in massive AGB stars than in low-mass stars, as seen in Fig. 8. However, the 3DUP and PM are complicated processes driven by convective motion, and could consequently be sensitive to local thermodynamic properties which are obviously expected to vary with stellar mass and metallicity (in this case, $\lambda_{\rm pm}$ and $\lambda_{\rm dup}$ would be Z- or M-dependent). For this reason, there is, so far, no theoretical evidence for any correlation between the stellar mass and metallicity and the efficiency of the PM mechanisms, and more particularly, no definite physical reason to believe that low-mass AGB stars are more efficient than high-mass stars in producing heavy nuclei.

Hot bottom burning (Scalo et al. 1975) plays an important role only in its possible impact on the ^{19}F destruction through the $^{19}\mathrm{F}\,(\mathrm{p}\,,\alpha)\,^{16}\mathrm{O}$ reaction. We refer to Mowlavi et al. (1996) who found that the ^{19}F destruction factor roughly amounts to about 1% per interpulse in a $6\,\mathrm{M}_\odot$ star of solar metallicity. Hot bottom burning has no effect on the s-process abundances.

5. Uncertainties in the s-process strength

The main uncertainties concern the quantitative determination of the 3DUP and PM characteristics which are expected to be sensitive to the stellar properties (such as the mass, metallicity, pulse number or mass loss rate) or the numerical prescriptions used. Within the framework of the parametric approach followed here, the impact of some known uncertainties, such as those affecting the nuclear reaction rates or the initial proton profile in the PM zone, on the s-process nucleosynthesis can be analysed.

5.1. Uncertainties of nuclear reaction rates

All results presented so far are based on the so-called "recommended" NACRE nuclear reaction rates. The impact of the nuclear uncertainties on the predicted light element yields resulting from the H- and He-burnings has already been discussed in detail by Arnould et al. (1999) in the framework of a parametric one-zone model. Nuclear, astrophysics and observational uncertainties and their influences on the s-abundance distribution have been studied by Goriely (1999) in the framework of the parametric canonical multi-event model. However, it remains unknown to what extent the s-process taking place in AGB stars could be affected by nuclear reaction rates uncertainties.

For each reaction, NACRE provides a recommended "adopted" rate, along with realistic lower and upper limits. For neutron capture reactions, only the uncertainty in the important $^{14}\mathrm{N}\,(\mathrm{n}\,,\mathrm{p})\,^{14}\mathrm{C}$ reaction is considered. The experimental determinations of Koehler & O'Brien (1989) (used in the previous sections) and Brehm et al. (1988) (which differ by a factor of about 2) are taken as upper and lower limits, respectively. To study the impact of the nuclear uncertainties on the s-process efficiency in AGB stars, the network calculations are reiterated by combining in many different ways the lower and upper limits of all the NACRE and $^{14}\mathrm{N}\,(\mathrm{n}\,,\mathrm{p})\,^{14}\mathrm{C}$ reaction rates.

[6] The data of Table 1 correspond to surface abundances of intrinsic AGB stars, since some long-lived radioactive nuclei such as ^{93}Zr ($\tau_{1/2} = 1.5\ 10^6$ yr) have not have time to totally decay yet. Extrinsic AGB stars would display different Nb abundances.

[7] For the same reason, it is dangerous to deduce, theoretically or observationally, average light or heavy s-element abundances by considering a mean abundance of elements which do not have the same s-contribution to the solar system (see Sect. 6).

Table 1. Elemental overabundance ratio [el/Fe] in four AGB stars of different metallicities Z. For each metallicity, the first column (labelled "dup") corresponds to the [el/Fe] abundance in the dredged-up material, while the other three columns correspond to the surface abundances predicted after respectively 10, 30 and 50 dredge-ups.

	$Z = 0.018$				$Z = 0.008$				$Z = 0.004$				$Z = 0.001$			
Z	dup	10	30	50	dup	10	30	50	dup	10	30	50	dup	10	30	50
30	0.16	0.03	0.07	0.10	0.20	0.01	0.02	0.04	0.26	0.01	0.02	0.04	0.44	0.00	0.00	0.01
31	0.52	0.13	0.27	0.35	0.53	0.03	0.09	0.13	0.60	0.03	0.08	0.12	0.86	0.00	0.01	0.02
32	0.62	0.16	0.34	0.44	0.68	0.05	0.13	0.20	0.79	0.05	0.12	0.19	1.09	0.01	0.02	0.03
33	0.44	0.10	0.22	0.29	0.47	0.03	0.08	0.12	0.55	0.02	0.07	0.10	0.80	0.00	0.01	0.02
34	0.81	0.26	0.49	0.60	0.83	0.07	0.19	0.27	0.90	0.06	0.16	0.23	1.18	0.01	0.02	0.04
35	0.54	0.13	0.29	0.37	0.53	0.03	0.09	0.14	0.57	0.03	0.07	0.11	0.81	0.00	0.01	0.02
36	0.86	0.28	0.53	0.65	0.94	0.10	0.24	0.34	1.04	0.08	0.21	0.30	1.59	0.02	0.06	0.10
37	0.70	0.20	0.40	0.50	0.86	0.08	0.20	0.29	1.05	0.09	0.22	0.31	1.75	0.03	0.08	0.13
38	1.63	0.86	1.23	1.38	1.62	0.36	0.68	0.85	1.67	0.30	0.59	0.76	1.95	0.05	0.13	0.19
39	1.58	0.81	1.18	1.33	1.61	0.36	0.68	0.85	1.68	0.30	0.60	0.77	1.95	0.05	0.13	0.19
40	1.61	0.83	1.20	1.34	1.70	0.41	0.74	0.92	1.79	0.36	0.68	0.85	2.22	0.08	0.21	0.31
41	-0.07	0.27	0.82	1.07	-0.14	0.08	0.40	0.65	-0.27	0.06	0.34	0.57	-2.30	0.00	0.02	0.04
42	1.42	0.67	1.03	1.17	1.55	0.33	0.63	0.80	1.61	0.27	0.55	0.71	1.97	0.05	0.13	0.20
44	1.24	0.55	0.89	1.03	1.38	0.26	0.53	0.69	1.42	0.20	0.44	0.59	1.50	0.02	0.05	0.08
45	0.95	0.34	0.60	0.73	1.09	0.14	0.32	0.44	1.13	0.10	0.26	0.36	1.15	0.01	0.02	0.04
46	1.45	0.70	1.06	1.20	1.62	0.37	0.68	0.85	1.67	0.30	0.59	0.75	1.69	0.03	0.07	0.12
47	0.89	0.30	0.57	0.71	1.05	0.13	0.31	0.43	1.09	0.10	0.25	0.36	1.12	0.01	0.02	0.03
48	1.46	0.70	1.06	1.21	1.67	0.39	0.72	0.90	1.75	0.34	0.65	0.82	1.89	0.04	0.11	0.17
49	-0.14	-0.02	-0.05	-0.07	-0.17	0.00	-0.01	-0.02	-0.25	0.00	-0.01	-0.02	-0.23	0.00	0.00	0.00
50	1.56	0.79	1.16	1.31	1.82	0.50	0.86	1.04	1.89	0.42	0.76	0.95	2.12	0.07	0.18	0.27
51	1.20	0.50	0.83	0.96	1.48	0.29	0.57	0.74	1.55	0.24	0.50	0.66	1.79	0.03	0.09	0.14
52	1.07	0.41	0.71	0.84	1.38	0.24	0.50	0.65	1.43	0.19	0.42	0.56	1.67	0.02	0.07	0.11
53	0.63	0.17	0.35	0.44	0.93	0.09	0.23	0.33	0.97	0.07	0.18	0.27	1.18	0.01	0.02	0.04
54	1.05	0.40	0.69	0.82	1.41	0.26	0.53	0.68	1.48	0.21	0.45	0.60	1.70	0.03	0.07	0.12
55	1.03	0.38	0.67	0.79	1.45	0.27	0.54	0.69	1.53	0.23	0.47	0.62	1.69	0.03	0.08	0.12
56	1.58	0.81	1.18	1.33	2.26	0.84	1.26	1.46	2.34	0.76	1.17	1.37	2.50	0.15	0.35	0.48
57	1.38	0.64	0.99	1.13	2.18	0.77	1.18	1.38	2.28	0.70	1.11	1.31	2.41	0.12	0.30	0.42
58	1.35	0.62	0.96	1.10	2.36	0.92	1.35	1.55	2.53	0.92	1.35	1.55	2.67	0.20	0.45	0.60
59	1.02	0.38	0.67	0.79	2.02	0.64	1.03	1.22	2.15	0.60	0.99	1.19	2.21	0.08	0.21	0.31
60	1.03	0.39	0.68	0.81	2.14	0.74	1.15	1.34	2.33	0.75	1.16	1.36	2.30	0.10	0.25	0.36
62	0.70	0.20	0.40	0.50	1.81	0.48	0.84	1.03	2.02	0.51	0.88	1.06	2.12	0.07	0.18	0.26
63	0.15	0.02	0.06	0.08	1.10	0.14	0.32	0.44	1.32	0.15	0.35	0.48	1.42	0.01	0.04	0.07
64	0.47	0.11	0.24	0.31	1.54	0.32	0.62	0.79	1.79	0.36	0.69	0.86	1.88	0.04	0.11	0.17
65	0.25	0.05	0.12	0.16	1.25	0.19	0.41	0.55	1.50	0.22	0.47	0.62	1.61	0.02	0.06	0.10
66	0.46	0.11	0.24	0.31	1.56	0.33	0.63	0.80	1.79	0.36	0.69	0.86	1.90	0.04	0.12	0.18
67	0.22	0.04	0.10	0.13	1.24	0.19	0.41	0.55	1.47	0.21	0.45	0.59	1.60	0.02	0.06	0.10
68	0.44	0.10	0.22	0.29	1.60	0.35	0.67	0.84	1.84	0.39	0.72	0.90	1.98	0.05	0.13	0.20
69	0.38	0.08	0.19	0.25	1.50	0.30	0.59	0.75	1.71	0.32	0.62	0.79	1.89	0.04	0.11	0.17
70	0.69	0.19	0.39	0.49	1.95	0.59	0.97	1.16	2.24	0.67	1.08	1.27	2.37	0.11	0.28	0.40
71	0.41	0.09	0.20	0.27	1.61	0.37	0.68	0.85	1.89	0.42	0.76	0.95	2.05	0.06	0.16	0.23
72	0.78	0.24	0.46	0.57	2.10	0.71	1.11	1.31	2.37	0.78	1.20	1.40	2.52	0.16	0.36	0.50
73	0.61	0.16	0.34	0.43	1.96	0.59	0.98	1.17	2.22	0.66	1.06	1.25	2.36	0.11	0.27	0.39
74	0.71	0.21	0.41	0.51	2.14	0.74	1.15	1.34	2.45	0.85	1.28	1.48	2.51	0.15	0.35	0.48
75	0.20	0.04	0.09	0.12	1.55	0.33	0.63	0.80	1.90	0.43	0.77	0.96	1.91	0.04	0.12	0.18
76	0.15	0.02	0.06	0.09	1.24	0.18	0.40	0.54	1.58	0.26	0.53	0.69	1.64	0.02	0.07	0.11
77	-0.07	-0.01	-0.02	-0.04	0.58	0.04	0.10	0.16	0.87	0.06	0.15	0.22	0.96	0.00	0.01	0.02
78	0.15	0.03	0.07	0.09	1.06	0.13	0.30	0.42	1.37	0.17	0.39	0.52	1.48	0.02	0.05	0.08
79	0.13	0.02	0.06	0.08	1.14	0.15	0.34	0.47	1.43	0.19	0.42	0.56	1.53	0.02	0.05	0.08
80	0.58	0.15	0.32	0.40	2.08	0.69	1.09	1.28	2.46	0.86	1.29	1.49	2.55	0.16	0.38	0.52
81	0.31	0.06	0.15	0.21	1.87	0.53	0.91	1.11	2.32	0.74	1.16	1.37	2.26	0.09	0.23	0.34
82	0.14	0.02	0.06	0.08	1.72	0.43	0.77	0.94	2.91	1.26	1.71	1.92	3.74	0.91	1.35	1.56
83	0.00	0.00	0.00	0.00	0.30	0.01	0.04	0.06	2.03	0.51	0.88	1.07	3.44	0.65	1.06	1.27

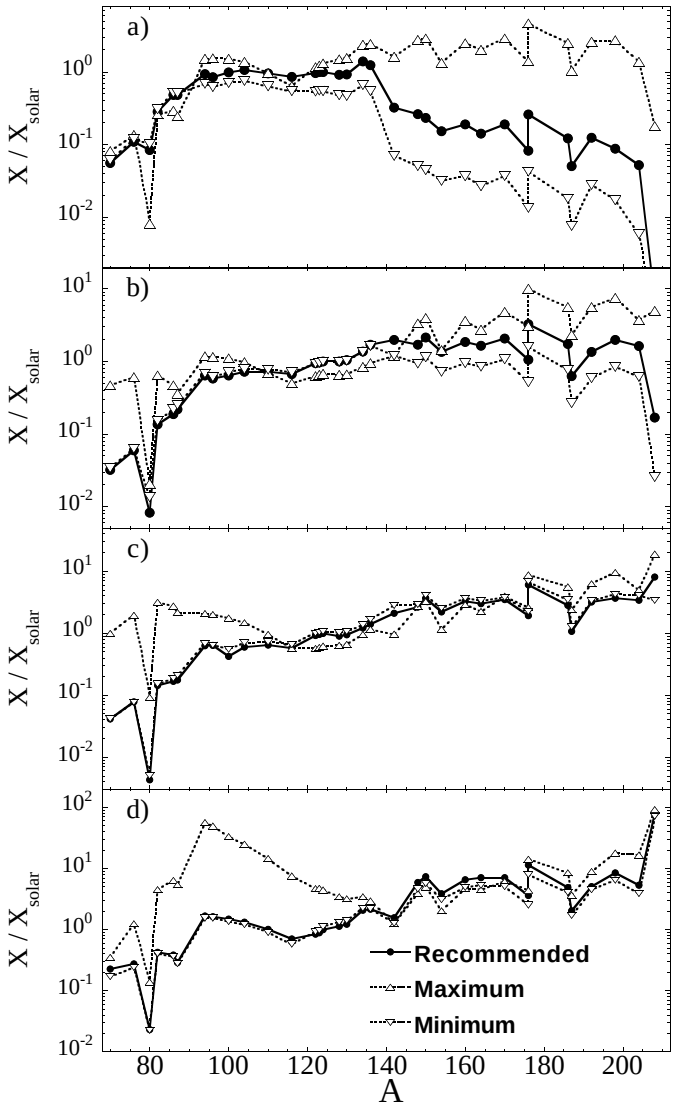

Fig. 9a–d. Surface overproduction factors (with respect to solar) of s-only isotopes after the onset of 30 dredge-ups in four AGB model stars. The full symbols correspond to the standard calculation obtained with the NACRE recommended rates. The triangle symbols correspond to the combination of upper and lower limits of NACRE and $^{14}\mathrm{N}\,(\mathrm{n}\,,\mathrm{p})\,^{14}\mathrm{C}$ rates leading to a minimum or maximum s-process strength. All curves are normalized to $X/X_{\odot}=1$ for ^{124}Te in the recommended case (the minimum and maximum curves are normalized accordingly). **a** corresponds to a $1.5\,\mathrm{M}_{\odot}$ $Z=0.018$ star, **b** to a $2.5\,\mathrm{M}_{\odot}$ $Z=0.008$ star, **c** to a $2.5\,\mathrm{M}_{\odot}$ $Z=0.004$ star and **d** and to a $3\,\mathrm{M}_{\odot}$ $Z=0.001$ star.

In solar metallicity stars, the remaining uncertainties in the reaction rates appear to be crucial for an exact determination of the s-abundance distribution. This is illustrated in Fig. 9a which shows surface overproduction factors for s-only isotopes with a combination of upper and lower limits of the rates leading to minimum or maximum s-process strength. The most critical reaction affecting the s-process strength are $^{13}\mathrm{C}\,(\mathrm{p}\,,\gamma)\,^{14}\mathrm{N}$ and $^{14}\mathrm{N}\,(\mathrm{n}\,,\mathrm{p})\,^{14}\mathrm{C}$. $^{13}\mathrm{C}\,(\mathrm{p}\,,\gamma)\,^{14}\mathrm{N}$ determines not only the amount of the neutron source ^{13}C left over in the PM zone, but also the amount of ^{14}N which is the major light neutron poison via $^{14}\mathrm{N}\,(\mathrm{n}\,,\mathrm{p})\,^{14}\mathrm{C}$. As a result, even the $\pm19\%$ uncertainty affecting the $^{13}\mathrm{C}\,(\mathrm{p}\,,\gamma)\,^{14}\mathrm{N}$ reaction rate at $T_8\simeq0.5$ can have a strong impact on the s-process, a larger rate strongly inhibiting the production of fresh ^{13}C. In addition, the resulting abundance of the major neutron poison ^{14}N can have drastic effects according to the adopted value of the still poorly known $^{14}\mathrm{N}\,(\mathrm{n}\,,\mathrm{p})\,^{14}\mathrm{C}$ rate. On the contrary, the s-process strength is almost totally insensitive to the uncertainties in the $^{13}\mathrm{C}\,(\alpha\,,\mathrm{n})\,^{16}\mathrm{O}$ rate. The neutron exposure is essentially a function of the total amount of fresh ^{13}C synthesized, and not of the rate at which it burns, since there is no competing channel during the He-burning.

In low-metallicity stars, the above-mentioned uncertainties become less relevant, because of the saturation of the number of neutrons captured at values around $n_{\mathrm{cap}}\simeq140$ (corresponding to the large production of Pb and Bi, the heaviest elements possibly produced), as seen in Fig. 2. However, the predictions become uncertain for metallicities below $Z=0.008$, because the high pulse temperatures characterizing those stars can lead to the activation of $^{22}\mathrm{Ne}\,(\alpha\,,\mathrm{n})\,^{25}\mathrm{Mg}$, the rate of which is still uncertain by a factor of about 100 at $T_8\simeq2.5$–3. For large values of that reaction rate (within the NACRE error bars), a weak s-process can take place during the convective pulse phase (Sect. 3), enabling the overproduction of $70\leq A\leq90$ s-elements[8] (Fig. 9d). These results are independent of the adopted value for the competing $^{22}\mathrm{Ne}\,(\alpha\,,\gamma)\,^{26}\mathrm{Mg}$ rate.

Regarding the production of ^{19}F in the PM zone, the remaining reaction rate uncertainties have a lower impact than for the s-process. This is due to the fact that the ^{19}F nucleosynthesis is favoured by large abundances of ^{13}C and ^{14}N and that $^{14}\mathrm{N}\,(\mathrm{n}\,,\mathrm{p})\,^{14}\mathrm{C}$ acts as a catalyst rather than a poison reaction (Arnould et al. 1999).

5.2. Uncertainties in the proton profile

So far, to simulate the s-process nucleosynthesis, we have adopted a so-called "standard" H abundance profile exponentially decreasing with depth and ranging from $X_{\mathrm{p}}^{\mathrm{mix}}=0.7$ at the bottom of the convective envelope to 10^{-6} at the bottom of the PM zone (the extent of which is fixed by the λ_{pm} parameter). However, the H profile might not follow an exponential law. We reiterate the nucleosynthesis calculations of Sect. 3 with modified initial H abundance profiles in the PM region, decreasing either faster or slower with depth than the standard case. These profiles are shown in Fig. 10, together with the range of $X_{\mathrm{p}}^{\mathrm{mix}}\simeq10^{-3}-10^{-2}$ where the s-process takes place (in low-Z stars, the region extends down to $X_{\mathrm{p}}^{\mathrm{mix}}=10^{-4}$, see Fig. 3). Only 5 to 20% (from the 'fast' to the 'slow' profiles, respectively) of the PM zone are seen to experience the s-process.

[8] Note that if ^{22}Ne burns at lower temperatures due to a larger $^{22}\mathrm{Ne}\,(\alpha\,,\mathrm{n})\,^{25}\mathrm{Mg}$ rate, the weak s-process is characterized by a low ^{80}Kr abundance, since the β-decay of ^{79}Se becomes too slow to feed ^{80}Kr during the neutron irradiation.

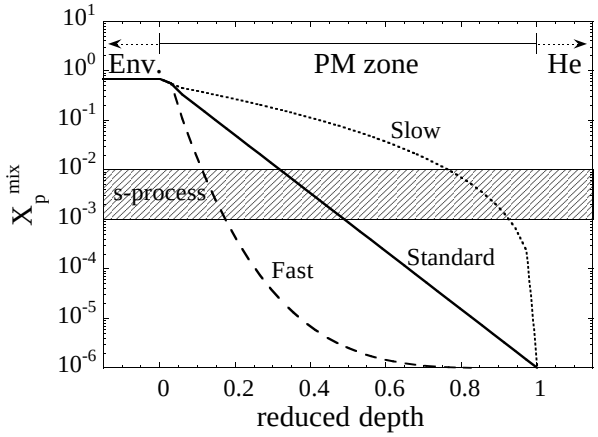

Fig. 10. Adopted H abundance profiles in the PM zone located between the stellar envelope and the He-burning shell. The standard case corresponds to the exponentially decreasing profile adopted, if no special reference is made. The shaded area corresponds to the major mass interval which experiences the s-process (cf Figs. 2-3). In the case of low-metallicity stars, this interval can extend down to $X_{\rm p}^{\rm mix} \sim 3\,10^{-5}$.

For $\lambda_{\rm pm} = 0.05$, this corresponds to a zone comprising some $10^{-5}\,{\rm M}_\odot$.

The surface overabundance predictions of the s-only nuclei resulting from those three initial H abundance profiles are shown in Fig. 11. Except for dilution effects (which slightly differ with the adopted profile), changing the H profile does not affect significantly the global s-abundance distribution. This is mainly due to the small range of $X_{\rm p}^{\rm mix}$ over which the s-process occurs. Only in the case of low-Z stars, a faster decreasing H profile favours a larger (with respect to the standard case) contribution from the $X_{\rm p}^{\rm mix} \simeq 10^{-4}$ range, and consequently a slightly greater production of $A \simeq 130$ nuclei.

The adopted initial H profile has a small impact on the qualitative production of ^{19}F which is synthesized over a small range around $3\,10^{-3} \lesssim X_{\rm p}^{\rm mix} \lesssim 3\,10^{-2}$. However, the production of F relative to s-process nuclei can differ depending on the adopted H-profile. In particular, a larger F to s-elements ratio is found for a 'slow' profile, as seen in Fig. 10 in the relative extent of the region covered by $3\ 10^{-3} \lesssim X_{\rm p}^{\rm mix} \lesssim 3\ 10^{-2}$ (responsible for the F production) and $10^{-3} \lesssim X_{\rm p}^{\rm mix} \lesssim 10^{-2}$ (responsible for the s-process).

The nucleosynthesis in the intershell region is affected quantitatively, but not qualitatively, by the still uncertain extent of the PM zone. Deeper in the intershell region, the temperature and density conditions increase, but the composition remains the same as in the upper part. Extending the PM zone deeper into the C-rich intershell does not affect qualitatively the nucleosynthesis related to the $^{12}{\rm C}\,({\rm p}\,,\gamma)\,^{13}{\rm N}$ or $^{13}{\rm C}\,(\alpha\,,{\rm n})\,^{16}{\rm O}$ reactions. Nevertheless, quantitatively, the stellar surface enrichment after a given thermal pulse cycle is directly proportional to the dilution factor $f_{\rm dil} = \lambda_{\rm pm} \times \lambda_{\rm dup} \times M_{\rm Pulse}\,/\,M_{\rm env}$. The $M_{\rm Pulse}/M_{\rm env}$ ratio is determined by evolutionary AGB models, but the extent of the 3DUP and PM zones are free parameters. Doubling the extent of the PM zone simply doubles the amount

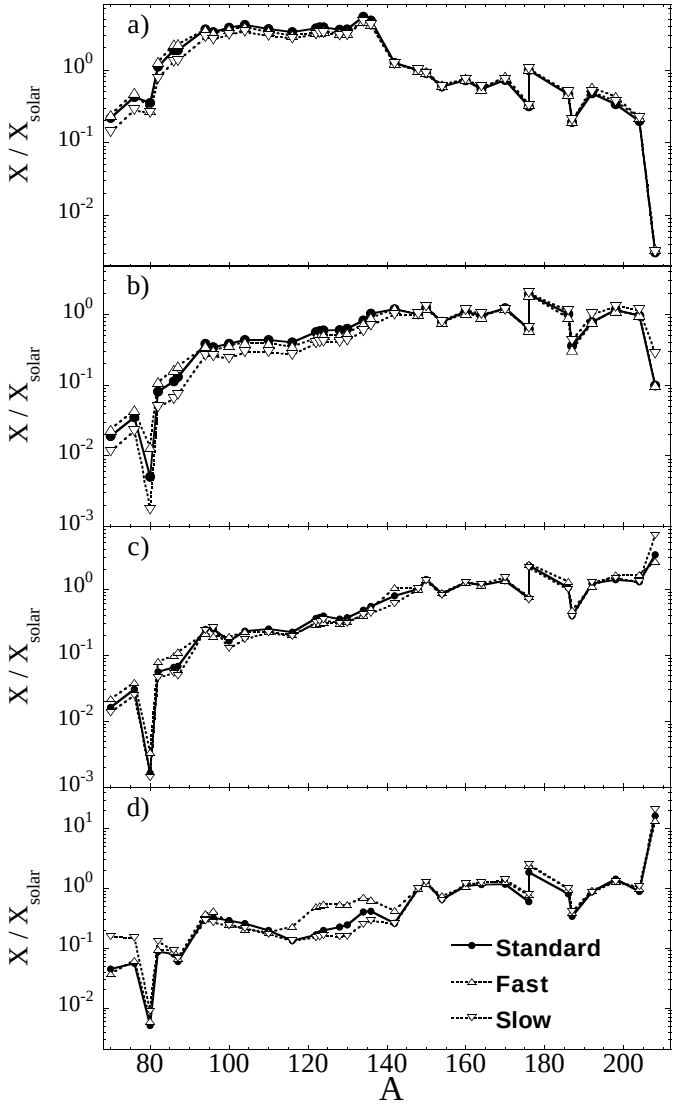

Fig. 11a–d. Same as Fig. 9 where the full symbols correspond to the calculation obtained with the standard H profile in the PM region, while the triangle symbols correspond to the fast and slow decreasing proton profiles shown in Fig. 10. All curves are normalized to $X/X_\odot = 1$ for ^{148}Sm.

of PM elements (in particular, ^{19}F, ^{23}Na and s-elements) ingested into the pulse-driven convective region. Increasing the 3DUP parameter affects not only the surface enrichment in PM elements, but also in all elements present in the He-flash region zone (in particular ^{12}C). The way the overall surface enrichment is affected by the adopted values of $\lambda_{\rm pm}$ is illustrated in Sect. 6.

In summary, qualitatively, the s-process predictions are only weakly dependent on the shape of the H-profile. On the other hand, the uncertain extent of the PM and DUP zones affects the quantitative surface enrichment.

6. Comparison with observational data

^{19}F and s-nuclei correspond to the best indicators to test the proton mixing into the C-rich zone.

6.1. Fluorine

Observations of fluorine abundances at the surface of giant stars are available, but restricted to stars with metallicities close to solar (Jorissen et al. 1992). A detailed comparison of those observations with abundance predictions from AGB models without PM has already been presented in Mowlavi et al. (1996) and showed the inadequacy of those models to account for the observed high F overabundances (^{19}F production is limited in those models by the abundance of secondary ^{13}C produced by the HBS). Including PM enables a much larger F enrichment of the stellar surface, as shown in Figs. 12-13. Yet, the F addition to the stellar envelope is predicted to be smaller than the C addition, so that only the less fluorine-enriched C stars can be explained. Larger surface content in F can be obtained but at the expense of a large pollution in ^{12}C, unless the PM zone is more extended and the DUP less efficient than assumed here. This feature holds true even if we double the F production in the intershell region, i.e taking $\lambda_{\rm pm} = 0.10$ (Fig. 12) or consider a slowly-decreasing H-profile which favours the production of ^{19}F. Diffusive overshooting at the bottom of the pulse-driven convective region can further increase the intershell ^{12}C (and consequently the surface) content (Herwig et al. 1999a). This puzzling feature is, however, sensitive to the still uncertain $^{12}\mathrm{C}\,(\alpha\,,\gamma)\,^{16}\mathrm{O}$ reaction rate. A faster rate would obviously reduce the surface ^{12}C to ^{16}O ratio at given surface ^{19}F enrichment. Another solution may come out from a better understanding of the structural evolution of those stars (PM, 3DUP, rotation)[9]. A firm conclusion cannot be drawn from our parametric PM calculations, but must wait for an consistent description of the time-evolution of the PM and 3DUP characteristics.

A clue in this respect is provided by the correlation observed between ^{19}F and s-nuclei overabundances (Jorissen et al. 1992). This correlation has already been successively studied by Mowlavi et al. (1998) in the framework of a parametric one-zone nucleosynthesis calculations. Our predictions (Fig. 13, where s-nuclei are traced by Zr) confirm that correlation, in good agreement with observations. This result is relatively insensitive to the adopted values of the PM and 3DUP parameters. Our PM model implies that protons are ingested into the C-rich layers at mass fractions covering the whole $X_{\rm p}^{\rm mix} \simeq 10^{-4} - 3 \times 10^{-2}$ range. Any explanation for the underabundant ^{19}F predictions relative to ^{12}C must take into account the correlation between ^{19}F and the s-process overabundances.

6.2. S-process elements

A widely used indicator of the neutron irradiation strength observed in s-process enriched objects is defined by the [hs/ls]-index, where the light s-element trace (the ls-index) is obtained by a mean of the Sr, Y and Zr abundances and the heavy s-element (hs-)index by the mean of the Ba, La, Nd and Sm (e.g Busso et al. 1999). Unfortunately, the definition of ls- and hs-indices differ from authors to authors. Elements characterized by a small s-contribution should be excluded in such estimates. In particular, the s-contribution to the solar abundance of Nd and Sm are predicted to be around 40 and 10%, respectively (Goriely 1999). Their elemental overabundance [el/Fe] is, therefore, expected to be smaller than for a pure s-process element, since the abundance is taken relative to the total solar abundance and not to the solar s-abundance. A mean hs-index including non major s-contributors is artificially reduced and can present a bias in the comparison of model and observation predictions. For this reason, we define here the hs-index as a mean of the Ba and La abundances. The predicted [hs/ls] index predicted in the framework of the present PM s-process model (Table 1) is shown in Fig. 14. Though it is usually believed that the [hs/ls] index increases with decreasing metallicities (due to the increase of the number of available neutrons to seed ratio), Fig. 14 clearly shows that the

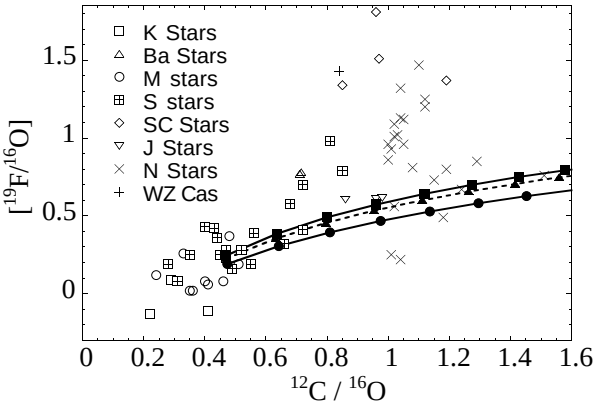

Fig. 12. Comparison of observations (Jorissen et al. 1992) with model predictions based on a $1.5M_{\odot}$ $Z = 0.018$ star. Each connected symbol corresponds to the enrichment due to a 3DUP episode, the nucleosynthesis in each interpulse-pulse sequence being taken identical. The calculated abundance ratios are obtained for $\lambda_{\rm dup} = 0.10$ and 2 sets of the PM parameters $\lambda_{\rm pm} = 0.05$ (circles) and $\lambda_{\rm pm} = 0.10$ (squares, triangles). The dashed line with triangles is obtained with the combination of upper and lower limits of the reaction rates leading to a maximum s-process strength (Fig. 9a).

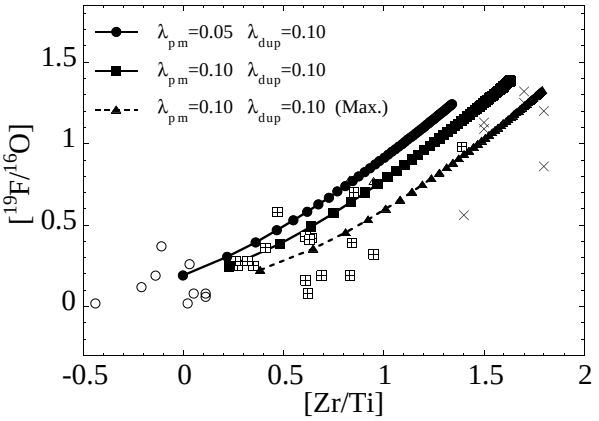

Fig. 13. Same as Fig. 12 for the ^{19}F and s-process correlation (Jorissen et al. 1992).

[9] It is unlikely that hot bottom burning may help predicting lower surface ^{12}C abundances at given ^{19}F abundance, since this process burns both ^{12}C and ^{19}F. Besides, most AGB stars are low-mass stars and are not expected to experience hot bottom burning.

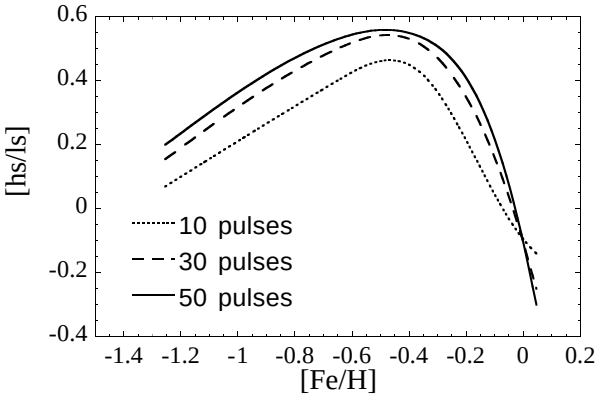

Fig. 14. Predicted [hs/ls] index as a function of the stellar metallicity [Fe/H] after the onset of a series of identical 10, 30 and 50 interpulse/pulse/dredge-up episodes. The calculations for the 5 model stars were performed with $\lambda_{\rm dup} = 0.10$ and $\lambda_{\rm pm} = 0.05$ (Fig. 8).

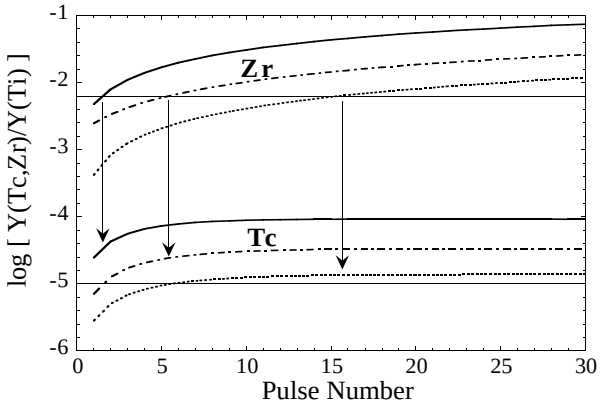

Fig. 15. Predicted abundances (relative to Ti) of Zr and Tc as a function of pulse number for $1.5M_\odot$ $Z = 0.018$ (full line), $2.5M_\odot$ $Z = 0.008$ (dash-dot line) and $3M_\odot$ $Z = 0.020$ stars. The thin horizontal lines correspond to a rough estimate of the detection threshold. The calculations were performed with $\lambda_{\rm dup} = 0.10$ and $\lambda_{\rm pm} = 0.05$.

[hs/ls]-index predicted by the partial mixing scenario presents a bell-shape as a function of metallicity. It should be recalled that the hs-index corresponds to s-abundances around Ba and that low metallicity stars tend to transform such elements in Pb, as clearly seen in Fig. 4. Our predictions are in qualitative agreement with the theoretical prediction shown in Fig. 16 of Busso et al. (1999), and with observations (Fig. 8 of Busso et al.), although some ambiguity arises from the definition of the hs-index.

The [hs/ls] index is sensitive to the initial stellar abundances of ^{12}C and light neutron poisons, as well as heavy nuclei. The efficiency of the PM of protons is also expected to be dependent on the stellar mass and pulse number. The large spread found in the observed [hs/ls]-index (Busso et al. 1999, Van Winckel & Reyniers 1999) indicates that nature is much more complex than the simple description given here.

Of particular interest is also the plateau behaviour predicted for the time evolution of the surface ^{99}Tc abundance, as shown in Sect. 4 (see also Smith and Wallerstein 1983, Busso et al. 1992). The surface Tc abundance obviously depends on the dilution of both the PM matter injected into the pulse and the dredged-up matter mixed in the envelope. Therefore, the absolute value of the ^{99}Tc plateau shown in Fig. 7 is directly proportional to the $\lambda_{\rm pm} \times \lambda_{\rm dup}$ product. The observation of Tc abundance in AGB stars could thus, in principle, constrain AGB model prescriptions regarding the extent of the 3DUP and PM zone. Unfortunately, both theoretical and observational uncertainties are large.

Another interesting information can be derived from the degree of detectability of various s-nuclei. As seen in Sect. 4, s-nuclei are produced in different amounts. As a result, some of them should become observationally detectable before others during the ascent of the AGB. An example is given in Fig. 15, where a rough estimate of the thresholds for Tc and Zr (Van Eck 1999, Vanture et al. 1991) is displayed together with surface abundance predictions. With these detection thresholds and model parameters, Tc should be observable after a few dredge-ups only, while Zr is expected to become detectable at a later stage (as shown by arrows in Fig. 15). This could explain the origin of the puzzling Tc-rich M stars (Van Eck 1999, Little-Marenin & Little 1987).

Finally, the standard PM scenario predicts that stars with metallicities $Z \lesssim Z_\odot/10$ should exhibit a large overproduction of Pb and Bi compared with other s-isotopes, in agreement with Gallino et al. (1998). Therefore, if the standard PM scenario holds, it should be possible to observe low-metallicity Pb-stars. Unfortunately, Pb detections are difficult and scarce in the literature. Gonzalez et al. (1998) detected the $\lambda 7228.97$ PbI line in FG Sge (but it appears blended with an unidentified neutral feature 0.1 Å bluewards), whereas the $\lambda 4057$ PbI line has been reported in Ap stars by Guthrie (1972). Sneden et al. (1996) attempted to detect the 3683.48 and 4057.82 PbI lines in the ultra-metal-poor star CS 22892-052, but failed to do so. More effort would be extremely useful for our understanding of the s-process in AGB stars. The Pb observation would be one of the clearest indicators of the PM mechanism and would strongly constrain s-process models. Inversely, if low-Z AGB stars enriched in s-process nuclei do not show any Pb overabundance, the standard PM scenario must be reviewed deeply.

7. Conclusions

Recent AGB studies, in particular models with diffusive overshooting or rotation, have improved the description of the PM of protons into the C-rich region. The crucial abundance profile of the protons mixed into the C-rich region is expected to be sensitive to the PM parameters (extent or efficiency of the overshooting, amplitude of the rotation). This leads to an uncertainty in the ^{13}C abundance profile after H-burning, and consequently, in the resulting s-process abundance distribution. The only way to handle this problem at the moment is to make fundamental assumptions regarding the proton abundance initially mixed into the C-rich layers. These crude approximations help us to understand the possible impact of the 3DUP and PM phenomena on the stellar surface enrichment. However, the simplified aspects

of the present calculations should be kept in mind, especially before drawing firm conclusions on the nucleosynthesis in AGB stars. In particular, there is, so far, no theoretical evidence about any correlation between the stellar mass/metallicity and the efficiency of the PM mechanism. For this reason, although low-M stars have larger pulse to envelope mass ratios compared with higher-M stars, it remains hazardous to conclude that low-mass AGB stars are the major contributors to the galactic enrichment in s-process nuclei.

Despite the above-mentioned shortcomings, the invoked 3DUP and PM mechanisms do have a strong impact on the nucleosynthesis in AGB stars. The operation of the 3DUP mechanism is of fundamental importance to explain the surface enrichment of light nuclei from C to Al and of the s-process elements, while the PM mechanism is essential in the production of ^{19}F and s-nuclei. Interestingly, the observed correlation between fluorine and s-process overabundances in AGB stars (Jorissen et al. 1992) provides some constraints on the PM mechanism. It requires that protons are injected into the C-rich layers at $X_{\rm p}^{\rm mix} \simeq 10^{-2}$ for the ^{19}F production and $X_{\rm p}^{\rm mix} \simeq 10^{-3}$ for the s-process nucleosynthesis. However, the relative surface enrichment in fluorine is predicted to be smaller than that of carbon, a theoretical issue which is difficult to reconcile with the observation of the largest F overabundances observed in N and SC stars.

Sodium is also predicted to be efficiently produced by the PM mechanism. While the mass extent over which that ^{23}Na is produced is small, its predicted mass fraction in the PM is up to fifty times higher than that left over by the hydrogen burning shell.

The abundance distribution of s-process elements principally depends on the PM characteristics and the stellar metallicity (the 3DUP efficiency only affects the dilution factor of the s-material into the envelope). The standard PM scenario predicts that AGB stars of metallicity close to solar produce elements in the $90 \leq A \leq 140$ mass range, while lower-metallicity stars ($Z \lesssim Z_{\odot}/2$) cover the production of nuclei in the larger $140 \leq A \leq 204$ range.

In addition, the standard PM scenario predicts that stars with metallicities $Z \lesssim Z_{\odot}/10$ should exhibit a large overproduction of Pb and Bi with respect to other s-isotopes. Therefore, if the standard PM scenario holds true, it should be possible to observe low-metallicity stars enriched in Pb (so-called 'Pb-stars'). Such an observation would be one of the clearest indicators of the PM mechanism and would strongly constrain s-process models. Inversely, if low-Z AGB stars enriched in s-process nuclei do not demonstrate an overabundance in Pb, the standard PM scenario must be reexamined deeply.

Important uncertainties remain in some nuclear reaction rates, namely in the $^{13}{\rm C}\,({\rm p}\,,\gamma)\,^{14}{\rm N}$, $^{14}{\rm N}\,({\rm n}\,,{\rm p})\,^{14}{\rm C}$ and $^{22}{\rm Ne}\,(\alpha\,,{\rm n})\,^{25}{\rm Mg}$ rates. New accurate measurements of these rates at energies of astrophysics relevance would be required to improve the nucleosynthesis predictions.

Another source of uncertainties concerns the extent and abundance profiles in the PM zone. However, our calculations show that the nucleosynthesis predictions are not strongly affected by the initial H abundance profile adopted as long as the H profile does not exhibit non-smooth behaviour in the small range around the proton-to-^{12}C abundance ratios of 0.1. In that case, the major uncertainty lies in the mass extent of the PM zone on which only stellar evolution calculations can shed light.

Within the PM model of the s-process, the solar distribution results from the chemical evolution of the Galaxy and not from successive neutron irradiations within a given stellar site (Travaglio et al. 1999). For this reason, the s-process nucleosynthesis (within the PM model), and more specifically the nucleosynthesis occurring around Pb, plays an important role in our understanding of the Galactic chemical evolution of nuclei heavier than iron. The s- and r-processes are known to be able to produce 100% of the solar system ^{208}Pb isotopes. However, their relative contributions remain ambiguous (Goriely 1999). Observing low-metallicity Pb-stars could shed light on the s-contribution to the solar abundance.

Acknowledgements. The authors are grateful to A. Jorissen, M. Arnould and S. Van Eck for helpful and stimulating discussions.

References

Angulo C., Arnould M., Rayet M., et al., 1999, Nucl. Phys. A656, 3
Arnould M., Goriely S., Jorissen A., 1999, A&A 347, 572
Asida S.M., Arnett D., 2000, ApJ, in press
Blöcker T., 1999, In: Le Bertre T., et al. (eds.) Proc. of the 191st IAU Symposium, Montpellier, France, PASP, p. 21
Boothroyd A.I., Sackmann I.-J., 1988, ApJ 328, 653
Brehm K., Becker H.W., Rolfs C., et al., 1988, Z. Phys. A 330, 167
Busso M., Gallino R., Lambert D.L., Raiteri C.M., Smith V.V., 1992, ApJ 399, 218
Busso M., Gallino R., Wasserburg G.J., 1999, ARA&A 37, 239
Clayton D.D., 1983, Principles of stellar evolution and nucleosynthesis. Univ. of Chicago Press
Frost C.A., Lattanzio J.C., 1996, ApJ 473, 383
Gallino R., Arlandini C., Busso M., et al., 1998, ApJ 497, 388
Gonzalez G., Lambert D.L., Wallerstein G., et al., 1998, ApJS 114, 133
Goriely S., 1999, A&A 342, 881
Goriely S., Mowlavi N., 2000, In: Noels A., et al. (eds.) Proc. of the 35th Liege International Astrophysics Colloquium, Université de Liege, p. 25
Guthrie B.N.G., 1972, Ap&SS 15, 214
Herwig F., Blöcker T., Schönberner D., El Eid M., 1997, A&A 324, L81
Herwig F., Blöcker T., Langer N., Driebe T., 1999a, A&A 349, L5
Herwig F., Blöcker T., Schönberner D., 1999b, In: Le Bertre T., et al. (eds.) Proc. of the 191st IAU Symposium, Montpellier, France, PASP, p. 41
Iben I. Jr., Renzini A., 1982, A&A 263, L23
Jorissen A., Arnould M., 1989, A&A 221, 161
Jorissen A., Smith V.V,, Lambert D.L., 1992, A&A 261, 164
Käppeler F., Beer H., Wisshak K., 1989, Rep. Prog. Phys. 52, 945
Koehler P.E., O'Brien H.A., 1989, Phys. Rev. C 39, 1655
Langer N., Heger A., Wellstein S., Herwig F., 1999, A&A 346, L37
Lattanzio J.C., 1998, In: Prantzos N., Harissopoulos S. (eds) Nuclei in the Cosmos. Editions Frontières, p. 163
Lattanzio J.C., Forestini M., 1999, In: Le Bertre T., et al. (eds.) Proc. of the 191st IAU Symposium, Montpellier, France, PASP, p. 31
Little-Marenin I.R., Little S.J., 1987, ApJ 93, 1539

Malaney R.A., 1987, Ap&SS 137, 251
Mowlavi N., 1995, Ph.D. Thesis, Université Libre de Bruxelles[10]
Mowlavi N., Jorissen A., Arnould M., 1996, A&A 311, 803
Mowlavi N., Jorissen A., Arnould M., 1998, A&A 334, 153
Mowlavi N., 1999a, A&A 344, 617
Mowlavi N., 1999b, A&A 350, 73.
Mowlavi N., Meynet G., 2000, In: Diehl R., Hartmann D. (eds.) Astronomy and Radioactivites. MPE Report, Munich, in press
Nemeth Zs., Käppeler F., Theis C., Belgya T., Yates S.W., 1994, ApJ 426, 357
Rayet M., Arnould M., Hashimoto M., Prantzos N., Nomoto K., 1995, A&A 298, 517
Scalo J.M., Despain K.H., Ulrich R.K., 1975, ApJ 196, 805
Smith V.V., Wallerstein G., 1983, ApJ 273, 742
Sneden C., McWilliam A., Preston G.W., et al., 1996, ApJ 467, 819
Takahashi K., Mathews G.J., Ward R.A., Becker S.A., 1986, In: Audouze J., Mathieu N. (eds.) Nucleosynthesis and its implications on nuclear and particle physics. D. Reidel Publishing, p. 285
Takahashi K., Yokoi K., 1987, At. Data Nucl. Data Tables 36, 375
Travaglio C., Galli D., Gallino R., et al., 1999, ApJ 521, 691
Van Eck S., 1999, Ph.D. Thesis, ULB (Belgium)
Vanture A.D., Wallerstein G., Brown J.A., Bazan G., 1991, ApJ 381, 278
Van Winckel H., Reyniers M., 1999, A&A in press

[10] Postscript file available by anonymous ftp on *obsftp.unige.ch* in *pub/mowlavi* or on the WWW at *http://obswww.unige.ch/~mowlavi/publications*.